NAVAL POSTGRADUATE SCHOOL
Monterey, California

AD-A252 936

DTIC
ELECTE
JUL 20 1992
S D

THESIS

OBSERVATIONS OF BREATHER SOLITONS

IN A NONLINEAR VIBRATORY LATTICE

by

Mary L. Atchley

March 1992

Advisor: Bruce C. Denardo
Co-Advisor: Steven L. Garrett

Approved for public release; distribution is unlimited.

92 7 1 050

92-19042

Unclassified

Security Classification of this page

REPORT DOCUMENTATION PAGE

1a Report Security Classification: Unclassified
1b Restrictive Markings:
2a Security Classification Authority:
3 Distribution Availability of Report: Approved for public release; distribution is unlimited.
2b Declassification/Downgrading Schedule:
4 Performing Organization Report Number(s):
5 Monitoring Organization Report Number(s):
6a Name of Performing Organization: Naval Postgraduate School
6b Office Symbol (If Applicable): PH
7a Name of Monitoring Organization: Naval Postgraduate School
6c Address (city, state, and ZIP code): Monterey, CA 93943-5000
7b Address (city, state, and ZIP code): Monterey, CA 93943-5000
8a Name of Funding/Sponsoring Organization:
8b Office Symbol (If Applicable):
9 Procurement Instrument Identification Number:
8c Address (city, state, and ZIP code):
10 Source of Funding Numbers:

Program Element Number	Project No	Task No	Work Unit Accession No

11 Title (Include Security Classification): Observations of Breather Solitons in a Nonlinear Vibratory Lattice

12 Personal Author(s): Mary Atchley

13a Type of Report	13b Time Covered		14 Date of Report (year, month,day)	15 Page Count
Master's Thesis	From	To	March 1992	84

16 Supplementary Notation: The views expressed in this thesis are those of the author and do not reflect the official policy or position of the Department of Defense or the U.S. Government.

17 Cosati Codes

Field	Group	Subgroup

18 Subject Terms (continue on reverse if necessary and identify by block number): Breather solitons

19 Abstract (continue on reverse if necessary and identify by block number)

Experimental, numerical, and analytical investigations of steady-state upper cutoff breather solitons in a one-dimensional lattice of coupled nonlinear oscillators are reported. These states are self-localized standing wave structures that can be considered as amplitude modulations of the upper cutoff mode, in which each oscillator is 180° out-of-phase with its immediate neighbors. The observation of the upper cutoff breather follows observations by previous investigators of the three other types of cutoff solitons: lower cutoff breathers, and lower and upper cutoff kinks. The experimental system is a lattice of magnetically coupled pendulums that is oscillated vertically. Numerical simulations are made in a lattice that approximately models the actual lattice. The structures are analytically described by a solution to a nonlinear Schrödinger equation supplemented with zero and second harmonics. The harmonic terms produce an antisymmetry in the breather amplitude profile that is noticeable in the experimental data and can be extreme in the numerical simulations. The theory completely fails in the extreme case, although the breather continues to exist.

20 Distribution/Availability of Abstract
[X] unclassified/unlimited [ ] same as report [ ] DTIC users

21 Abstract Security Classification: Unclassified

22a Name of Responsible Individual	22b Telephone (Include Area code)	22c Office Symbol
Bruce C. Denardo	(408) 646-3485	PH/De

DD FORM 1473, 84 MAR 83 APR edition may be used until exhausted
All other editions are obsolete

security classification of this page
Unclassified

Approved for public release; distribution is unlimited.

Observations of Breather Solitons in a Nonlinear Vibratory Lattice

by

Mary L. Atchley
B.S., University of California, Santa Cruz, 1986

Submitted in partial fulfillment of the requirements
for the degree of

MASTER OF SCIENCE IN PHYSICS

from the

NAVAL POSTGRADUATE SCHOOL
March, 1992

Author: Mary L. Atchley
Mary L. Atchley

Approved by: B. Denardo
Bruce C. Denardo, Advisor

Steven L. Garrett, Co-advisor

Karlheinz E. Woehler, Chairman, Department of Physics

ABSTRACT

Experimental, numerical, and analytical investigations of steady-state upper cutoff breather solitons in a one-dimensional lattice of coupled nonlinear oscillators are reported. These states are self-localized standing wave structures that can be considered as amplitude modulations of the upper cutoff mode, in which each oscillator is 180° out-of-phase with its immediate neighbors. The observation of the upper cutoff breather follows observations by previous investigators of the three other types of cutoff solitons: lower cutoff breathers, and lower and upper cutoff kinks. The experimental system is a lattice of magnetically coupled pendulums that is oscillated vertically. Numerical simulations are made in a lattice that approximately models the actual lattice. The structures are analytically described by a solution to a nonlinear Schrödinger equation supplemented with zero and second harmonics. The harmonic terms produce an antisymmetry in the breather amplitude profile that is noticeable in the experimental data and can be extreme in the numerical simulations. The theory completely fails in the extreme case, although the breather continues to exist.

Accession For
NTIS GRA&I ☑
DTIC TAB ☐
Unannounced ☐
Justification
By
Distribution/
Availability Codes
Dist | Avail and/or Special
A-1

TABLE OF CONTENTS

I. INTRODUCTION....1

II. THEORY....6

A. STANDARD LATTICE MODEL....6

B. DIPOLE LATTICE MODEL....11

III. EXPERIMENT....17

A. LATTICE APPARATUS....17

B. PROCEDURES....21

C. RESULTS....26

IV. NUMERICAL SIMULATION....29

A. PROGRAM DESCRIPTION....29

B. DRIVE PARAMETER PLANE....32

C. COMPARISON TO THEORY....35

V. CONCLUSIONS AND FUTURE WORK....41

APPENDIX A. SINGLE-OSCILLATOR THEORY....44

A. UNDRIVEN UNDAMPED CASE....44

B. DAMPED PARAMETRICALLY DRIVEN CASE....52

APPENDIX B. CIRCULARLY INTERRUPTED LATTICE.....58

APPENDIX C. BEAD LATTICE.....63

A. CONDITION FOR HARDENING.....63

B. CONDITION FOR GLOBAL PARAMETRIC DRIVE.....68

C. EXPERIMENT.....72

REFERENCES.....74

INITIAL DISTRIBUTION LIST.....77

ACKNOWLEDGMENTS

I wish to express my appreciation to the many people who helped make this work possible. Foremost, I would like to thank my advisor, Dr. Bruce Denardo, for his guidance and patience throughout this research. I would also like to thank Jay Adeff for his photography expertise, and David Gardner for his help with the accelerometer. I would also like to acknowledge Andrés Larraza, Chip McClelland, Colin Cooper, and Glenn Harrell for their invaluable contributions.

I. INTRODUCTION

Finite amplitude wave motion can exhibit behavior that is fundamentally different from linear motion. For example, in systems with little or no dispersion, nonlinearities can cause a wave to evolve into a series of shock fronts. By "dispersion" is meant that monochromatic waves of different frequencies travel at different speeds. A wave packet, which is composed of a band of frequencies, will thus spread or "disperse." Nonlinearity and dispersion thus compete against each other. It is possible to have a balance between the two effects, leading to a stable localized wave of constant profile, or a soliton. The first observation of such a wave was in a canal in 1834 (Dodd et al. 1982). It was not until the second half of this century that another remarkable property was discovered: solitons collide elastically (Zabusky and Kruskal 1965). This was surprising because collisions between nonlinear waves typically produce other waves, whose frequencies are the sum and difference of the frequencies of the incoming waves.

Although there is now a large body of theoretical literature on solitons, experimental observations are not abundant (Christiansen 1988) and applications are still under development. One application is in fiber optic communications, where the self-localized nature of solitons offers the possibility of fast "clean" digital information transfer (Mollenauer 1991). It is also possible that solitons are utilized in some biological systems as a means of energy transport (Davydov 1985), although this has not been proven.

One type of soliton may arise when a weakly nonlinear slowly-varying amplitude modulation of a wave is considered. The resultant equation for the modulation is nearly always a "nonlinear Schrödinger" (NLS) equation, which has this name because it is similar to the quantum mechanical Schrödinger equation for the wavefunction Ψ with an additional term proportional to $|\Psi|^2\Psi$. The fiber optic solitons are of the NLS type, as are certain types of localized

standing waves. The subject of this thesis is one such standing wave soliton.

To understand these solitons, consider an infinite one-dimensional uniform lattice of linearly coupled oscillators. The system is undriven and undamped. The oscillators are assumed to be nonlinear (App. A); specifically, they are either "soft" (the frequency decreases as the amplitude is increased) or "hard" (the frequency increases as the amplitude is increased). For example, a lattice of coupled pendulums is a softening system. It is convenient to represent standing wave motions of the lattice by arrows which show the peak-to-peak amplitudes and phases of the oscillators. Fig. I.1 shows the lower and upper cutoff standing wave modes of the lattice. Because the coupling is effectively absent in the lower cutoff mode, its linear frequency is less than the linear frequency of the upper cutoff mode. For linear motion, the frequencies of all other modes lie between the linear frequencies of the cutoff modes. For finite-amplitude motion, fundamentally new structures can occur (Fig. I.2). These are localized states which can be considered as amplitude modulations of the cutoff modes. They are examples of solitons. Two types can occur: breathers and kinks. To understand the first, consider the softening lower cutoff case. The frequency is below the linear lower cutoff frequency as a result of the finite-amplitude motion in the body of the breather. In the wings, where the motion is linear, energy can therefore not propagate outward; the wings are evanescent tails. The breather is thus a self-trapped state. Essentially the same argument applies to the upper cutoff breather, which exists at a frequency above the linear upper cutoff frequency. This state is quantitatively treated in Ch. II. The kinks exist at frequencies in the linear frequency band. Their explanation is different from that for breathers, and is given by Denardo (1990).

The first observation of a standing wave soliton was by Wu et al. (1984) who observed a lower cutoff breather as a steady state cross surface wave in a vertically oscillated channel of deep liquid. The theory, which yielded an NLS equation, was subsequently established by Larraza and Putterman (1984a and

1984b) and independently by Miles (1984). Softening breathers and softening kinks were later observed in a pendulum lattice by Denardo (1990). The observation of this kink motivated the discovery of the analogous lower cutoff kink in a channel of shallow liquid (Denardo et al. 1990). All of these observations were not difficult. The observation of the remaining soliton, the upper cutoff breather, was the primary goal of this thesis.

The observation of the upper cutoff breather was difficult. The first attempt, which predated our work by several years, was made by Denardo who attached rubber bands to the bottoms of the pendulums in his lattice. The other ends of the rubber bands were attached to a rod directly below and parallel to the lattice. This arrangement caused the oscillations to harden. The failure to observe an upper cutoff breather was attributed to nonuniformity of the rubber bands. Springs were then attempted, but failed for the same reason. The attempts described here dealt with three candidate systems: a magnetically coupled pendulum lattice (Ch. III), an interrupted pendulum lattice (App. B), and a lattice of beads on a string (App. C). Initial attempts with each of these systems failed. Success occurred only after a *refined* magnetically coupled pendulum lattice was constructed.

To confirm that the observed localized structures were indeed upper cutoff breathers, we conducted numerical investigations of a system that models the actual lattice (Ch. IV). It was here that we first observed a dramatic and unexpected antisymmetry in the structure of the breather. This prompted us to include dc and second harmonic effects in the theory (Sec. II.B), which at least qualitatively agree with the observations at low amplitudes.

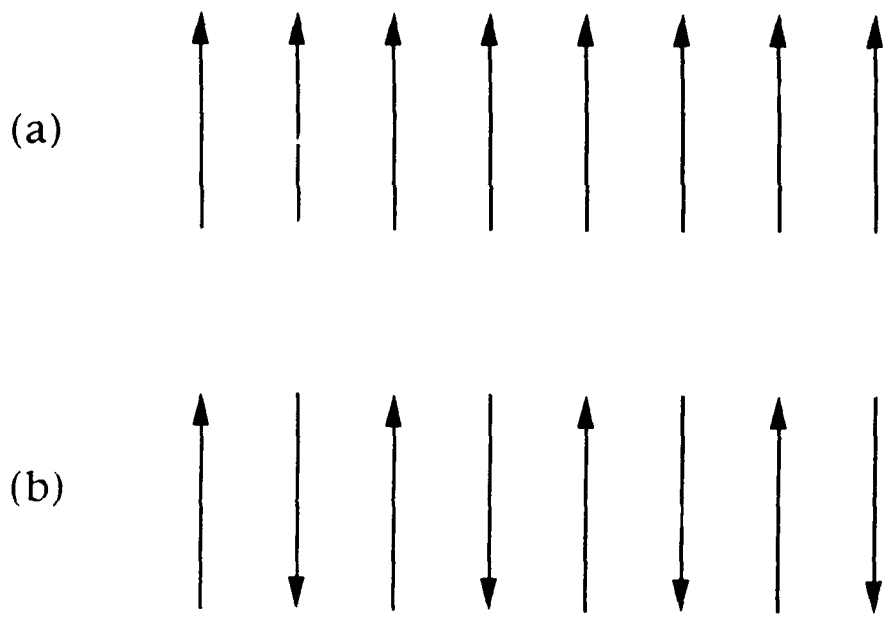

Fig I.1 Representations of the (a) lower cutoff mode, and (b) upper cutoff mode of a lattice of coupled oscillators. The arrows correspond to the peak-to-peak amplitudes and phases of the oscillators.

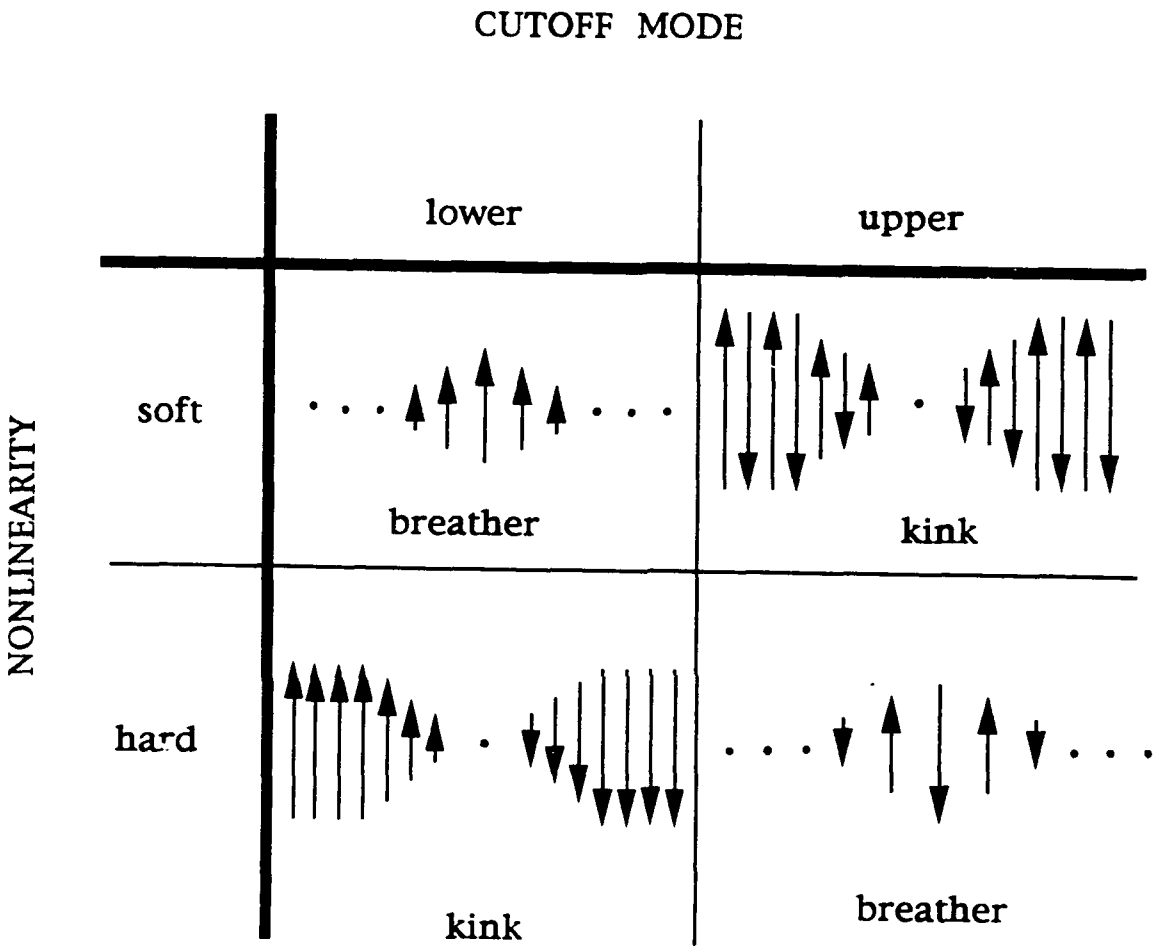

Fig. I.2 Classification of NLS standing wave solitons.

II. THEORY

The motion of a plane pendulum, and the generalization to a broad class of single-degree-of-freedom nonlinear oscillators, is considered in App. A. In this chapter, we analytically investigate the motion of a lattice of coupled nonlinear oscillators. We begin with the simplest undriven undamped case in Sec. II.A, in order to establish the method. A model of our actual lattice, which is more complicated and includes drive and dissipation, is then investigated in Sec. II.B. In both cases, we obtain a localized nonpropagating breather solution.

II.A. STANDARD LATTICE MODEL

Consider the lattice of coupled plane pendulums in Fig. II.A.1. The motion of the pendulums is transverse. The coupling is linear and exists only between nearest neighbors. We define μ to be the coupling constant between two adjacent pendulums (μ is the proportionality constant that gives the torque in terms of the difference in the angles of the pendulums). The torque on the n^{th} pendulum is

$$\tau_n = \mu(\theta_{n+1} - 2\theta_n + \theta_{n-1}) - mgL\sin\theta_n , \qquad \text{(II.A.1)}$$

where the last term is due to the gravitational restoring force. Equating the torque to the product of the moment of inertia and the angular acceleration gives

$$I\ddot{\theta}_n = \tau_n , \qquad \text{(II.A.2)}$$

where $I=mL^2$ is the moment of inertia. Substituting (II.A.1) into (II.A.2), we obtain

$$\ddot{\theta}_n - \frac{\mu}{I}(\theta_{n+1} - 2\theta_n + \theta_{n-1}) + \omega_o^2 \sin\theta_n = 0\,, \qquad \text{(II.A.3)}$$

where $\omega_o^2=g/L$. For weakly nonlinear motion, we can expand $\sin\theta_n$ in a power series and neglect all terms of higher order than cubic. Then (II.A.3) becomes

$$\ddot{\theta}_n - \frac{\mu}{I}(\theta_{n+1} - 2\theta_n + \theta_{n-1}) + \left(\frac{2\mu}{I} + \omega_o^2\right)\theta_n = \alpha\theta_n^3\,. \qquad \text{(II.A.4)}$$

where the nonlinear coefficient is $\alpha = \omega_o^2/6$ for the pendulum lattice. We generalize (II.A.4) by allowing α to be an independent parameter which can be positive (softening) or negative (hardening). We refer to the lattice corresponding to (II.A.4) as the "standard" model.

We now consider the upper cutoff mode (Fig. II.A.2a) and assume the amplitude to be weakly nonlinear and slowly-varying in both space and time:

$$\theta_n(t) = (-1)^n A(na,t)e^{i\omega t} + \text{c.c.} + (\text{harmonics})\,, \qquad \text{(II.A.5)}$$

where a is the lattice spacing, c.c. denotes the complex conjugate, and A(na,t) is a complex function that is slowly-varying in both space and time. Substituting (II.A.5) into (II.A.4) and neglecting the higher harmonics because they are small, we obtain

$$\ddot{A} + 2i\omega\dot{A} + \frac{\mu}{mL^2}[\,A((n+1)a,t) + A((n-1)a,t)]$$

$$+\left(\frac{2\mu}{mL^2} + \omega_o^2 - \omega^2\right)A = 3\alpha|A^2|A\,. \qquad \text{(II.A.6)}$$

Because we have assumed that A is slowly-varying with respect to time, we can neglect the second time derivative compared to the first time derivative. By

adding and subtracting $2\mu A(na,t)/I$ to the left hand side of the above equation, we can approximate the third term as the second derivative of A with respect to space. That is,

$$A((n+1)a,t) - 2A(na,t) + A((n-1)a,t) \cong a^2 \frac{\partial^2}{\partial x^2} A(na,t) , \qquad \text{(II.A.7)}$$

where x is the position along the lattice. Eq. (II.A.6) then becomes a nonlinear Schrödinger (NLS) equation for the upper cutoff mode:

$$2i\omega A_t + c^2 A_{xx} + (\omega_1^2 - \omega^2) A = 3\alpha |A^2| A , \qquad \text{(II.A.8)}$$

where $\omega_1^2 = 4\mu/I + \omega_0^2$ is the square of the linear frequency of the upper cutoff mode and $c^2 = \mu a^2/I$. The subscripts of A in (II.A.8) denote partial derivatives.

For $\alpha < 0$ (hardening) and $\omega > \omega_1$ there exists a time-independent localized solution (Denardo 1990) to the NLS equation (II.A.8) :

$$A(x) = \left[\frac{2(\omega^2-\omega_1^2)}{-3\alpha}\right]^{\frac{1}{2}} \operatorname{sech}\left[\left(\frac{\omega^2-\omega_1^2}{c^2}\right)^{\frac{1}{2}}(x-x_o)\right] . \qquad \text{(II.A.9)}$$

Hence, the envelope of the upper cutoff mode is exponentially localized. The motion of the lattice is represented in Fig. II.A.2b. This is referred to as a breather soliton in the upper cutoff mode, and was explained physically in Ch. I. According to the NLS theory, the midpoint x_0 can occur anywhere along the lattice. Note that the product of the width $[c^2/(\omega^2-\omega_1^2)]^{1/2}$ and the amplitude $[2(\omega^2-\omega_1^2)/(-3\alpha)]^{1/2}$ is independent of the frequency ω. Hence, as ω is increased, the soliton amplitude increases and the characteristic width decreases.

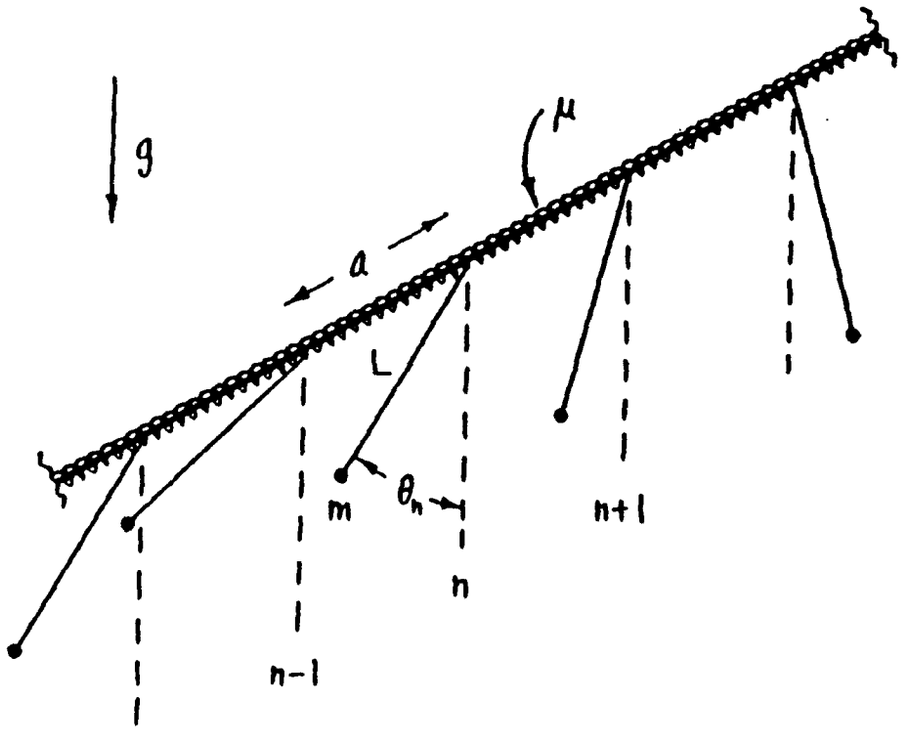

Fig. II.A.1 Pendulum lattice. The motion is purely transverse, and the coupling is linear.

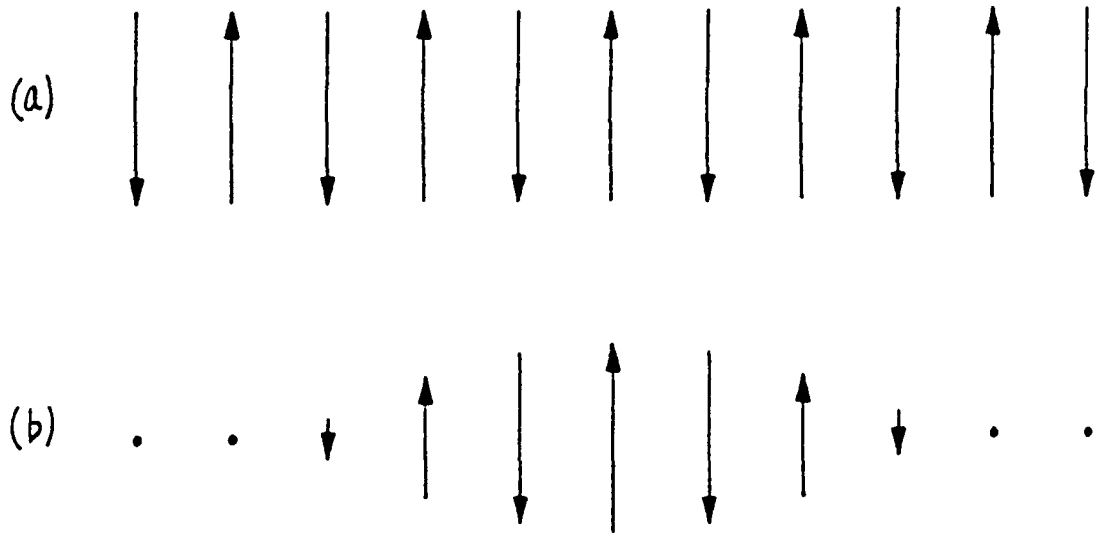

Fig. II.A.2 Upper cutoff motion of a hardening lattice:
(a) uniform state, and (b) breather.

II.B. DIPOLE LATTICE MODEL

For an upper cutoff breather to exist in a lattice, the upper cutoff mode must harden (Sec. II.A). We have constructed a system that has this property. It is a longitudinal lattice of pendulums that are coupled magnetically (Sec. III.A). The purpose here is to abstract from the actual lattice a simple model that can be readily handled analytically, and to obtain an upper cutoff breather solution.

The model is represented in Fig II.B.1. We assume point dipoles, and include only nearest-neighbor interactions. (This is a reasonable approximation because next-nearest-neighbor interactions in a pure upper cutoff mode cancel by symmetry.) Each dipole sits in an external gravitational potential well. The equilibrium lattice spacing is taken to be unity. The coupling is assumed to be substantially stronger than the gravitational forces, so that the nonlinearity arising from the latter is negligible. The equation of motion for the displacement θ_n of the n^{th} oscillation is thus

$$\ddot{\theta}_n + \beta\dot{\theta}_n + \omega_o^2 [1 + 2\eta\cos(2\omega t)]\,\theta_n + \frac{\mathcal{C}^2}{16}\left[\frac{1}{(1+\theta_{n+1}-\theta_n)^4} - \frac{1}{(1+\theta_n-\theta_{n-1})^4}\right] = 0\,, \qquad \text{(II.B.1)}$$

where we have included linear damping and parametric drive of the gravitational force. The drive amplitude is 2η, the drive frequency is 2ω, and the damping coefficient is β. On the weakly nonlinear level, we can make the approximation

$$\frac{1}{(1+x)^4} \cong 1 - 4x + 10x^2 - 20x^3\,. \qquad \text{(II.B.2)}$$

We first consider the pure upper cutoff mode ($\theta_{n+1} = -\theta_n$) on the linear level with no drive and no dissipation. Equation (II.B.1) then becomes

$$\ddot{\theta}_n + (\omega_o^2 + c^2)\theta_n = 0 \ , \qquad \text{(II.B.3)}$$

from which we identify the linear frequency ω_1 of the mode:

$$\omega_1^2 = \omega_o^2 + c^2 \ . \qquad \text{(II.B.4)}$$

The factor of 1/16 was inserted in (II.B.1) so that no constant factors would occur in the expression (II.B.4).

To third order, the equation of motion (II.B.1) becomes

$$\ddot{\theta}_n + \beta\dot{\theta}_n + \omega_o^2 (1 + 2\eta\cos 2\omega t)\, \theta_n - \frac{c^2}{4}(\theta_{n+1} - 2\theta_n + \theta_{n-1})$$

$$+ \alpha (\theta_{n+1} - \theta_n)^2 - \alpha (\theta_n - \theta_{n-1})^2 - \gamma (\theta_{n+1} - \theta_n)^3 + \gamma (\theta_n - \theta_{n-1})^3 = 0 \, , \qquad \text{(II.B.5)}$$

where $\alpha = \frac{5}{8}c^2$ and $\gamma = \frac{5}{4}c^2$. We consider an amplitude modulation of the upper cutoff mode:

$$\theta_n = (-1)^n A(n,t)e^{i\omega t} + (-1)^n B(n,t)e^{3i\omega t} + \text{c.c.} + \ldots$$

$$+ C(n,t)e^{2i\omega t} + \text{c.c.} + D(n,t) + \ldots \ , \qquad \text{(II.B.6)}$$

where the amplitudes are in general complex. The ellipsis in (II.B.6) represents higher harmonics. The following perturbation regime is assumed:

$$|A| \approx \varepsilon << 1 \qquad |A_x| \approx \varepsilon^2, \qquad |A_t| \approx \varepsilon^3,$$
$$|B|, |C|, |D| \approx \varepsilon^3, \qquad \omega\beta, \eta \approx \varepsilon^2 \, , \qquad |\omega^2 - \omega_1^2| \approx \varepsilon^2 , \qquad \text{(II.B.7)}$$

where the x and t subscripts denote partial differentiation. (We have replaced n by a continuous variable x.) Substituting (II.B.6) into the equation of motion

(II.B.5), neglecting terms of order higher than ε^3, and equating to zero the coefficients of $e^{i\omega t}$, $e^{3i\omega t}$, $e^{2i\omega t}$, and e^0, we obtain the following relations:

$$2i\omega A_t + (\omega_o^2 + c^2 - \omega^2 + i\omega\beta)A + \frac{c^2}{4}A_{xx} + \omega_o^2\eta A^* + 48\gamma|A|^2A = 0 \qquad \text{(II.B.8)}$$

$$B = \frac{16\gamma}{9\omega^2 - \omega_o^2 - c^2} A^3 \qquad \text{(II.B.9)}$$

$$C = \frac{8\alpha}{4\omega^2 - \omega_o^2} AA_x \qquad \text{(II.B.10)}$$

$$D = -\frac{8\alpha}{\omega_o^2} (AA_x^* + A^*A_x) \ . \qquad \text{(II.B.11)}$$

These equations are accurate to order ε^3. The assumed orders in (II.B.7) lead to the NLS-plus-harmonics description in (II.B.8)-(II.B.11). This description will not hold if the actual powers of ε differ from those in (II.B.7).

The nonpropagating single-breather solution is

$$A = Ae^{i\delta} , \qquad \text{(II.B.12)}$$

where

$$A = \frac{\mu}{2\sqrt{6\gamma}} \operatorname{sech}\left[\frac{2\mu}{c}(x - x_o)\right] \qquad \text{(II.B.13)}$$

$$\tan(2\delta) = -\frac{\omega\beta}{\nu} \qquad \text{(II.B.14)}$$

$$\nu = \sqrt{\omega_o^4\eta^2 - \omega^2\beta^2} \qquad \text{(II.B.15)}$$

$$\mu = \sqrt{\omega^2 - \omega_o^2 - c^2 + \nu} \ . \qquad \text{(II.B.16)}$$

In (II.B.13), the location x_o of the breather is arbitrary. The displacement (II.B.6) is

$$\theta_n = (-1)^n 2A\cos(\omega t + \delta) + (-1)^n 2B\cos(3\omega t + 3\delta) + 2C\cos(2\omega t + 2\delta) + D\,, \qquad \text{(II.B.17)}$$

where

$$B = \frac{16\gamma}{9\omega^2 - \omega_o^2 - c^2} A^3 \qquad \text{(II.B.18)}$$

$$C = \frac{8\alpha}{4\omega^2 - \omega_o^2} AA_x \qquad \text{(II.B.19)}$$

$$D = -\frac{16\alpha}{\omega_o^2} AA_x \qquad \text{(II.B.20)}$$

Note that C (second harmonic amplitude) and D (dc amplitude) are of opposite sign and thus competition arises between the two corresponding terms. However, $|D| > 4|C|$, so the dc term dominates the second harmonic term.

The turning points corresponding to (II.B.17) are in general difficult to determine (Denardo 1990). However, if B, C, and D are sufficiently small compared to A, which fortunately turns out to be the case in our numerical simulations (Sec. IV.C), then the turning points occur simply when $\cos(\omega t+\delta)$ is an extremum. The maximum and minimum displacements are then

$$\theta_{max} = 2A + 2B + 2C + D \qquad \text{(II.B.21)}$$

and

$$\theta_{min} = -2A - 2B + 2C + D\ . \qquad \text{(II.B.22)}$$

The general profile of the motion is sketched in Fig. II.B.2. It can be considered as a skewed hyperbolic secant. Motion to the right in the lattice is displayed in the upward direction on the graph, and motion to the left is displayed in the downward direction. Thus there is a net force away from the center of the soliton in both directions, resulting in the asymmetry of the profile. The force is a result of the dc term in (II.B.6), and is analogous to radiation pressure in acoustics.

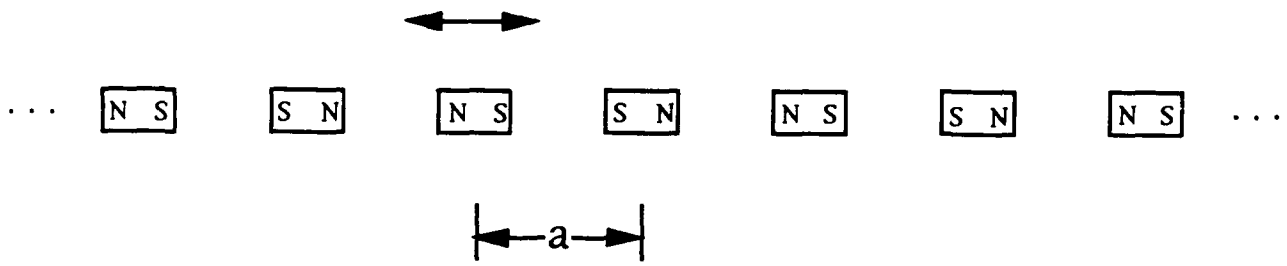

Fig. II.B.1 Dipole lattice model. The motion is longitudinal.
Each dipole sits in an external potential well (not shown).

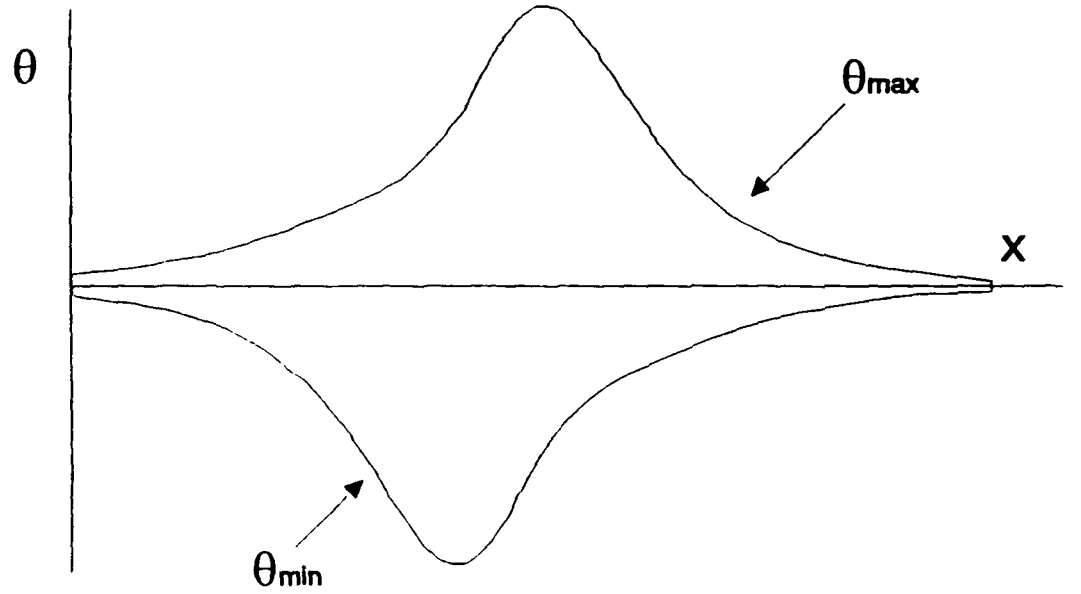

Fig. II.B.2 General analytical profile of the dipole lattice breather in the upper cutoff mode.

III. EXPERIMENT

To observe an upper cutoff breather soliton, we require a lattice whose upper cutoff mode hardens. Three such systems were initially considered: (a) a magnetically coupled pendulum lattice that was obtained commercially, (b) an interrupted pendulum lattice, and (c) a lattice of beads on a string. Fig. III.A.1 shows lattice (a), which was purchased from Fisher Scientific Co. (stock #S42170) who advertises it as a traveling wave demonstration apparatus. Lattice (b) was the softening pendulum lattice of Denardo (1990) modified with circular interrupters along the length in order to harden the oscillations. Lattice (c) consisted of lead fishing sinkers equally spaced on nylon fishing line. Lattices (b) and (c) are described in Apps. B and C, respectively. Lattices (a) and (b) were driven globally by a vertical shake table, and lattice (c) was longitudinally driven at one end. All attempts to observe an upper cutoff breather in these lattices failed. The occurrence of transverse motion in (a) prompted us to design and construct a lattice in which this was not allowed. The resultant lattice, which was successful, is the subject of this chapter.

III.A. LATTICE APPARATUS

To restrict the motion to be only longitudinal, a lattice was constructed with rigid pendulums pivoted at their tops (Fig. III.A.2). This was the idea of modelmaker G. Harrell, who also built the lattice. It consists of a wooden platform and back supporting an aluminum bar. The platform has holes to secure it to the shake table. The aluminum bar has threaded holes at intervals of 1/8" for stainless steel 4-40 cap head screws to support the individual pendulums. The spacing of the pendulums can thus be changed in 1/8" increments. We performed our investigations with a total of 23 pendulums

equally spaced a distance of 1.25 inches. The pendulums are made of plexiglass with dimensions of 3.5" X 3/4" X 3/16". They are rectangular except for a tapering in the width at the top. The width tapers to 1/4" in the top 3/4" of the length of the pendulum. At the top of each pendulum is a hole for the cap head screw. At the bottom of each pendulum is a 7/16" diameter hole to hold the magnet. The magnets are NdFeB, with a thickness of 1.67 mm and with a hole of diameter 3.51 mm. Each adjacent pendulum is oriented so that like polarities face each other, creating a repulsive force between adjacent pendulums. Otherwise, the equilibrium configuration (in which all the pendulums are hanging vertically) is unstable.

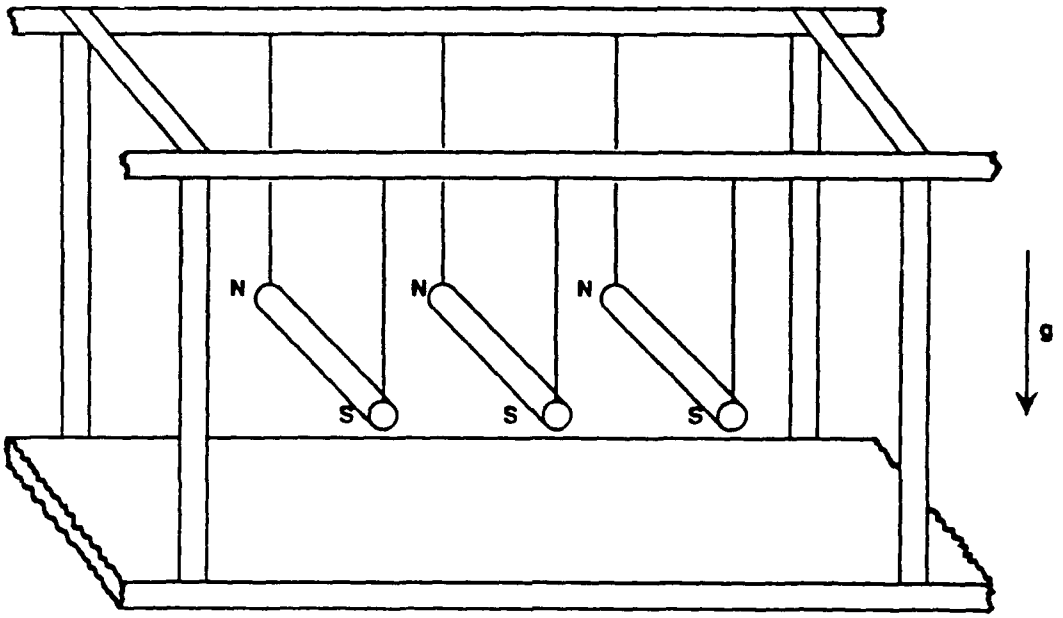

Fig. III.A.1 Section of the magnetically coupled pendulum lattice from Fisher Scientific Co.

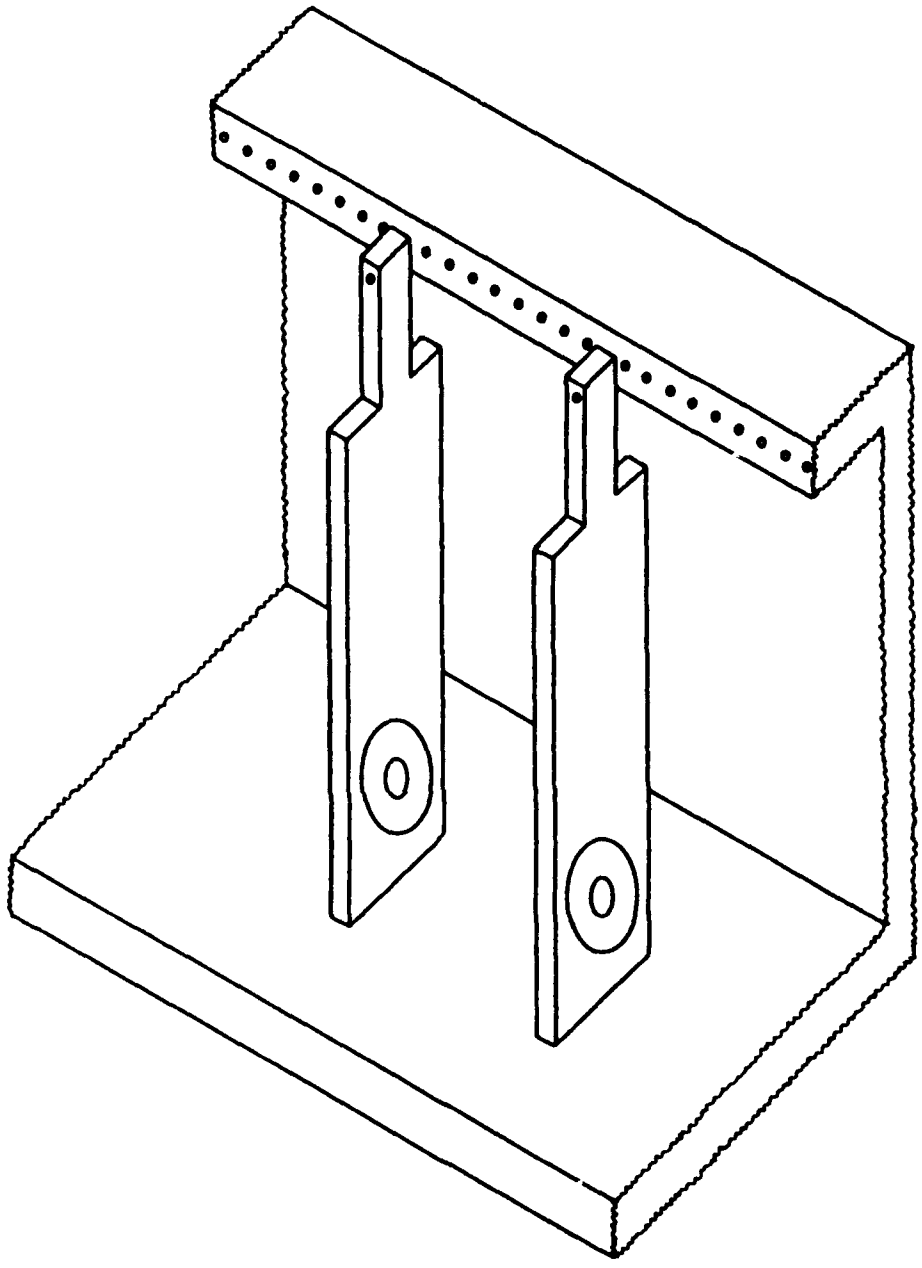

Fig. III.A.2 Section of our magnetically coupled pendulum lattice.

III.B. PROCEDURES

The maximum amplitude on both sides of equilibrium of each pendulum was determined photographically with the help of J. Adeff. A strobe was set to fire at either the frequency of the drive or the frequency of the response, depending on whether we wanted one or both turning points in the photograph. It was necessary to find a way to frequency-lock the strobe and the drive, and to adjust the relative phase such that the strobe fired when the pendulums were at maximum amplitude. A block diagram of the set-up is shown in Fig. III.B.1. The HP3314 Function Generator was set to a square wave in the BST ("burst") mode, N cycle (N=1), and externally triggered by the HP3325B Synthesizer, which was driving the shake table at 11.0 Hz and 1.2 V_{pp}. The SYNC signal from the synthesizer is seen on the oscilloscope. The frequency of the function generator must be greater than that of the synthesizer in order to lock onto the trigger. The strobe must have at least 5 volts amplitude to trigger, and it triggers on one of the edges of the square wave from the function generator. By varying the frequency of the function generator, it can be seen on the oscilloscope that the strobe is being triggered at various phases of the drive. By setting the function generator to 1/2 cycle, the strobe is being triggered at the response frequency. The frequency of the function generator is kept constant at some convenient value. By setting the PHASE of the function generator and adjusting the SYMmetry, the pendulums can be seen to first increase and then decrease in amplitude as the SYM is changed in one direction. In this way, the strobe was set to fire when the pendulums had reached their maximum amplitudes. By toggling the trigger slope button on the function generator, a 180^{o} phase shift is obtained, and the other turning point of the pendulums can be seen.

The measurements were taken by projecting the photographic slide onto a large piece of white paper taped to the wall. The horizontal support rod

and the pivot points of each pendulum were traced. The midpoint of the bottom segment of each pendulum was marked with a ruler. The pivot point and the point marked at the bottom of the pendulum was then connected by a line. It was confirmed (by eyeball) that the line drawn was parallel to the edges of the pendulum. Another line was drawn from the pivot point perpendicular to the support rod, and the angle between the two lines was measured.

The only significant sources of error occur in measuring the angle and in locating the center of the bottom segment of each pendulum. Because these sources are independent, they add in quadrature. A conservative estimate of ± 0.25° was made for locating the center and ± 0.1° in measuring the angle. The uncertainty of the angular displacement of each pendulum is thus

$$\delta\theta = \pm\sqrt{(0.25)^2 + (0.1)^2} \cong \pm 0.27^\circ \cong \pm 0.005 \text{ radians.} \qquad \text{(III.B.1)}$$

The peak-to-peak displacement of the shake table driven by the HP 3325B Synthesizer was determined with an ENDEVCO 2215E accelerometer. The sensitivity of this particular accelerometer is 187.3 pC/g. The accelerometer was mounted to the lattice on the shake table and its output measured as a function of drive amplitude at a frequency of 11.3 Hz. This frequency was chosen because it is the same frequency at which the photographs were taken for the profile data. The capacitance of the accelerometer plus cable was measured to be 10.68 nanofarads. The output of the accelerometer was conditioned by an Ithaco 1201 Low Noise Preamplifier which has an input impedance of 100 MΩ. The 11 Hz signal was thus well above the -3 dB roll-off frequency ($1/2\pi RC$ = 0.15 Hz). A plot of accelerometer output vs. drive amplitude is shown in Fig. III.B.2 for the fundamental frequency and the second and third harmonics. The output is linear over a wide range of drive amplitude. Note that the third harmonic becomes large at high drive amplitude. The accelerometer output was checked by measuring its output for

two fixed points: 1 g peak (where g is the acceleration due to gravity) and 10 m/s^2 RMS. The 1 g point was found by simply placing a small piece of brass rod on the shake table and increasing the drive amplitude until it began to rattle. The rattle point was more easily seen by putting the accelerometer output through an oscilloscope, where spikes appear in the output when the object begins to rattle. The accelerometer output measured produced a value of 9.84 m/s^2, in good agreement with the accepted value, 9.80 m/s^2. The other fixed point was measured using a Brüel & Kjaer Type 4294 Calibration Exciter. This device vibrates at a frequency of 159.2 Hz (10^3 rad/sec) and an acceleration of 10 m/s^2 RMS. The accelerometer output gave a value of 9.98 m/s^2 RMS, in good agreement.

The manufacturer's sensitivity and the relation Q=CV yielded a calibration constant of 1.79 $mV/(m/s^2)$. The accelerometer output at a drive of 11.3 Hz and 1.2 V_{p-p} (the parameters at which the profile data was obtained) measured 6.99 mV RMS. Dividing this by the calibration constant yielded an acceleration of 3.9 m/s^2 RMS. Using the relation $x=a/\omega^2$, we obtained an RMS displacement of 0.77 mm, which corresponds to a peak-to-peak displacement of 2.18 mm.

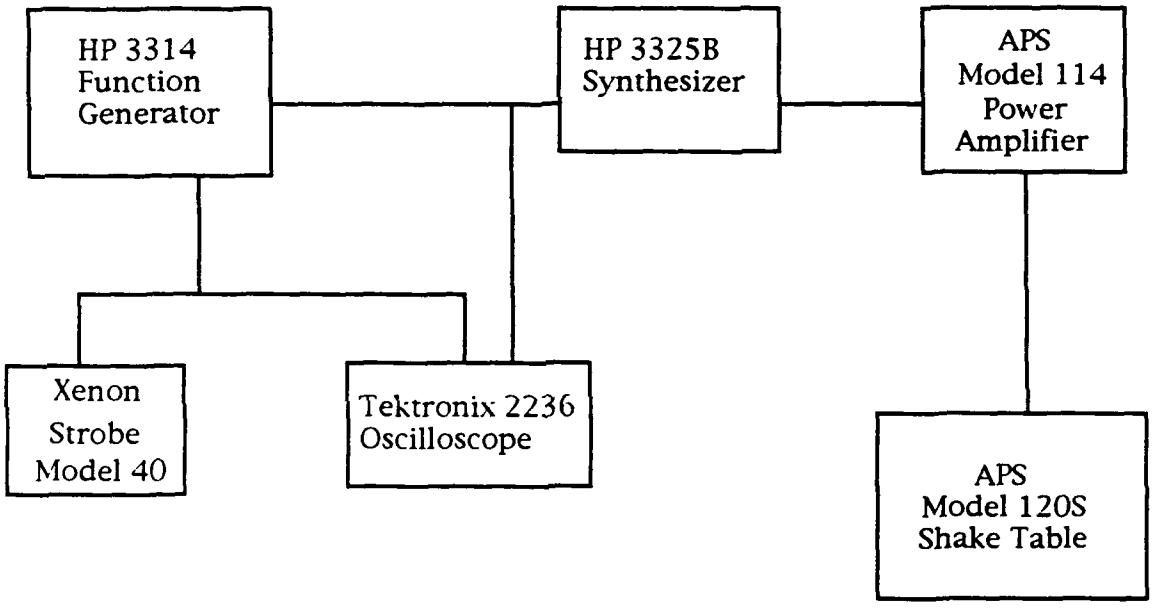

Fig. III.B.1 Block diagram of the experimental apparatus.

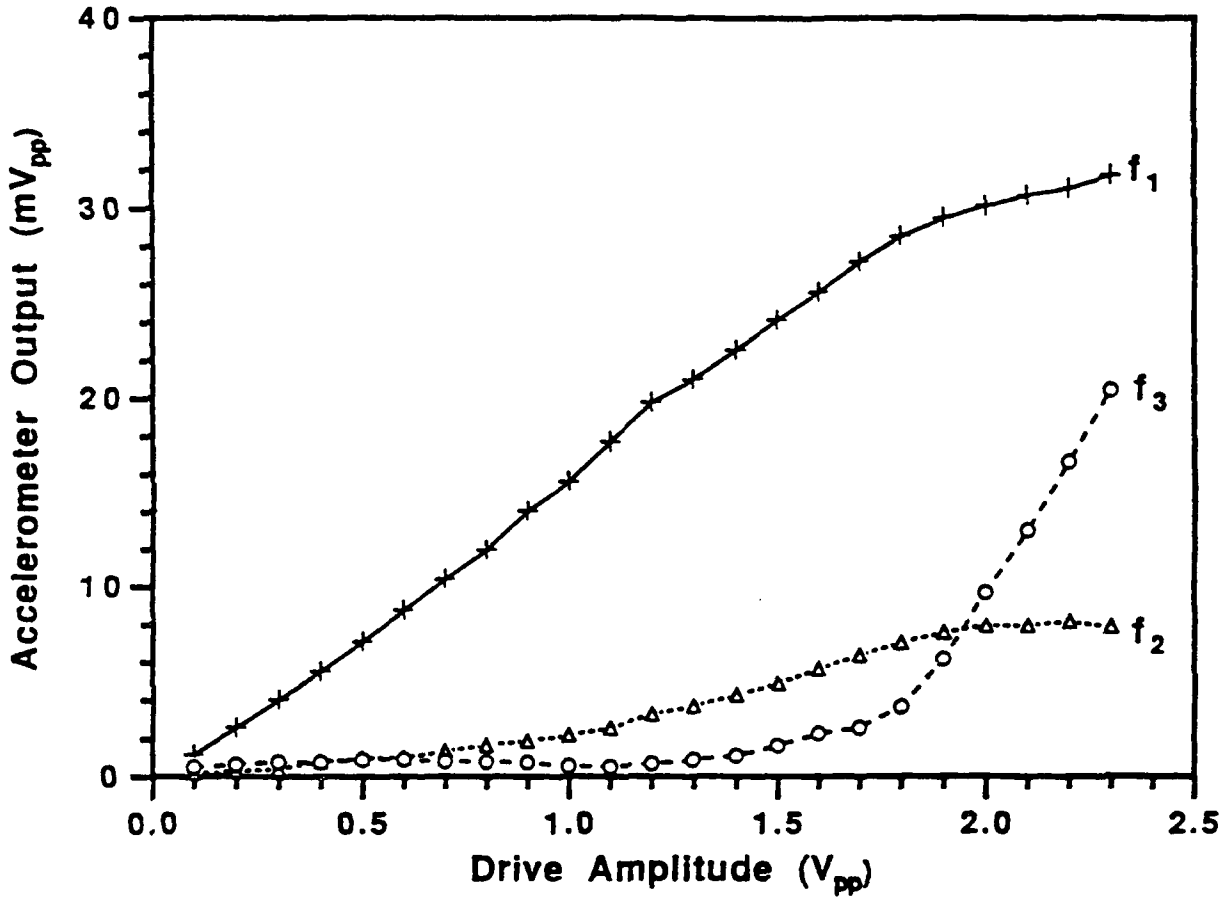

Fig. III.B.2 Accelerometer output vs. drive amplitude at a drive frequency of 11.3 Hz. f_1 is the fundamental frequency, f_2 and f_3 are the second and third harmonics, respectively.

III.C. RESULTS

Steady-state experimental data is shown in Fig. III.C.1, for drive frequency 11.3 Hz and peak drive amplitude 1.08 mm. The crosses represent the turning point displacements at one time, and the boxes at a time differing by one half cycle. The uncertainty (III.B.1) of the amplitudes is ± 0.005 rad, which accounts for part of the scatter of the data. The remainder is presumably a result of nonuniformities. Pendulums 1-6 and 17-23 were at rest within the uncertainty of our measurements. Many or perhaps all of these pendulums may have been exactly at rest due to static friction.

The structure in Fig. III.C.1 is clearly localized, and has the appearance of an upper cutoff breather soliton. To obtain this state, we typically perturb four of the pendulums so that each is 180° out-of-phase with its immediate neighbors. The motion can then evolve into the localized structure. We have observed these states at different locations on the lattice, although certain locations were found to be preferable. Typically, a localized structure would form at one location and then drift to the location shown in Fig. III.C.1. This is presumably due to nonuniformities in the lattice.

We slowly varied the drive parameters after a localized structure was obtained, in order to observe changes in the profile. We found that the profile did not change substantially before instabilities occurred. At a drive amplitude of 1.2 Vp-p, quasiperiodicity occurred at roughly 11.5 Hz. At lower frequencies (roughly 10.3 Hz) the system decayed to rest.

The asymmetry between the two turning point displacements of each pendulum is clearly evident in Fig. III.C.1. Specifically, the amplitude away from the center of the structure is greater than the amplitude toward the center. This "radiation pressure" is predicted by the theory (Sec. II.B) which, to lowest order, gives a profile of the form

$$y_{\pm} = \pm A \text{ sech}[\kappa(x - x_0)] + B \text{ sech}^2[\kappa(x - x_0)] \tanh[\kappa(x - x_0)] , \qquad \text{(III.C.1)}$$

where y_+ and y_- are the positive and negative turning point displacements, respectively. For simplicity, we have neglected a sech^3 term in (III.C.1). An eyeball best fit of (III.C.1) to the experimental data is shown in Fig. III.C.1. The values of the parameters are A=0.115, B=0.085, κ=0.55, and x_0=11.0. The fit is in qualitative agreement with the experimental data.

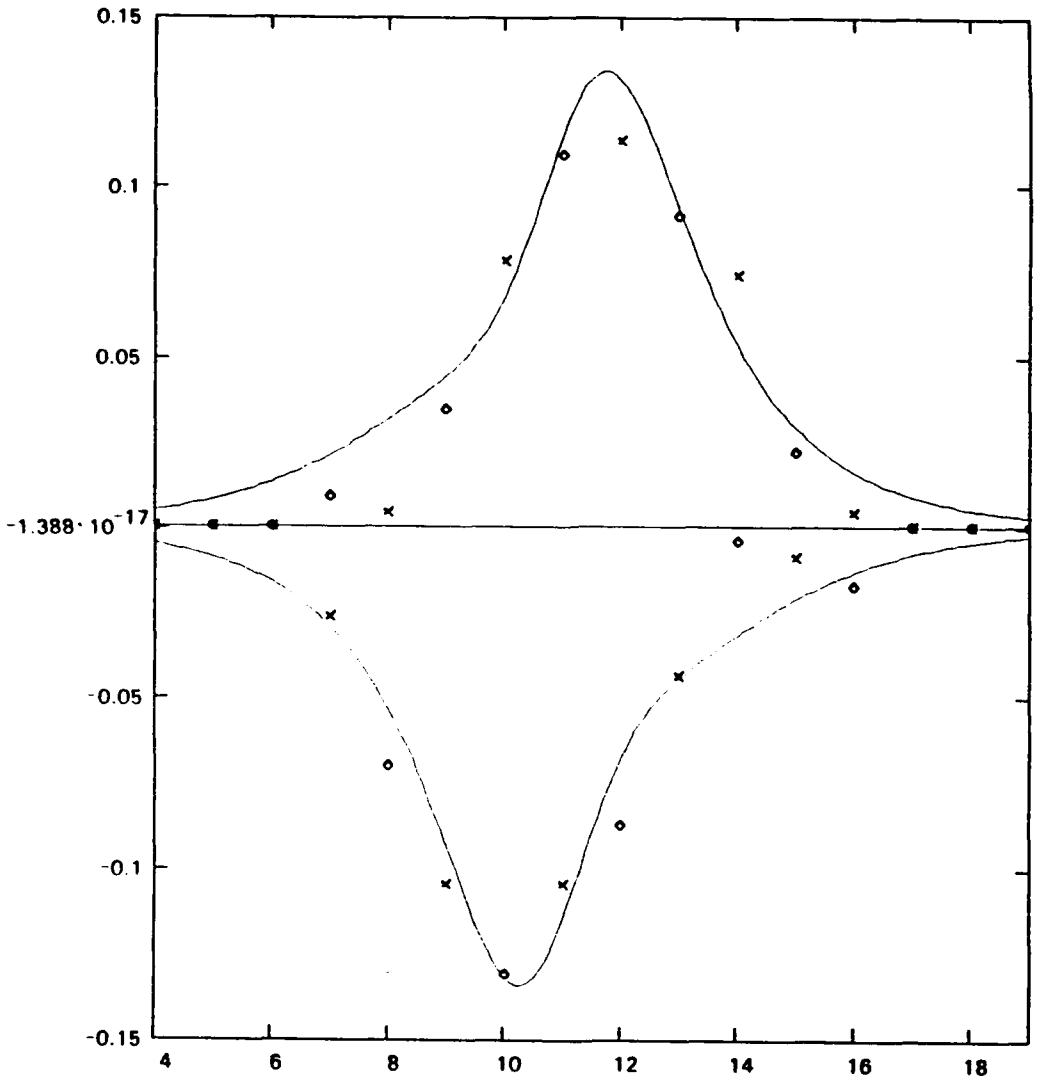

Fig. III.C.1 Upper cutoff breather in the magnetically coupled lattice. The points are experimental; the curves are a best-fit based on the theory.

IV. NUMERICAL SIMULATION

Our theoretical (Ch. II) and experimental (Ch. III) investigations do not conclusively establish the existence of upper cutoff breathers. The theoretical investigations are insufficient because a stability analysis is not included. (Such an analysis appears to be very difficult to perform.) In the experiment, one could argue that the observed structure is merely a linear localized standing wave which is trapped on a nonuniformity (Feynman et al. 1965). In order to confirm the existence of upper cutoff breathers, and to more readily probe their properties, we conducted numerical investigations of the model lattice (Sec. II.B).

The computer program is described in Sec. IV.A. The breather was found to exist and be stable for a range of drive parameters (drive amplitude and frequency). This region in the "drive plane" is discussed in Sec. IV.B. Numerical breather "profiles" (or sets of lattice site amplitudes near turning points of the motion) are compared to theory in Sec. IV.C.

IV.A. PROGRAM DESCRIPTION

The program was written by a previous student (Galvin 1990) and later modified by another student (Walden 1991), and was run on a Dell 486 - 33 MHz computer. The program uses the equation of motion (II.B.1), which includes terms for damping and parametric drive to yield steady-state motion of the lattice. All parameters are scaled to be dimensionless. The boundary conditions are periodic.

The computer monitor displays dots representing the instantaneous locations of the individual lattice sites. Only the center 40 dots are displayed,

although up to 150 lattice sites can be used. The lattice sites are counted from right to left. Although the motion in the magnetic lattice is longitudinal, it is represented on the monitor as transverse so that the profile and fine motion can be more easily observed. Upward motion on the computer display corresponds to a pendulum moving to the right, and downward motion to the left. The user can interactively change the drive amplitude, drive frequency, or damping with a keystroke, in a coarse or fine increment. The coarse increment is ten times the fine increment. The maximum amplitude can also be displayed with a keystroke.

The initial conditions specify the position and velocity of each lattice site. Constant parameters such as coupling and damping must also be specified. Existing files can be used for the initial conditions, or one can create new files. The user specifies the time step to be used, which is equal to the number of steps per period of response calculated by the computer.

The program also allows the user to zoom in or zoom out, with regard to the scale of the motion. This function changes the vertical scale by a factor of two, but leaves the horizontal scale unchanged. Zooming in allows the user to see small-scale motion which is not otherwise apparent.

Steady-state motion of the system is checked roughly by choosing a particular element of the lattice to monitor. This element is shown by a different dot color. The computer measures 20 successive peaks of this element, takes their average, and checks whether each peak is within 1% of the average. If so, then the system is considered to be in the steady state. The computer informs the user that the element has passed the check by reversing the colors of the lattice dots. This check is useful but not entirely valid. For example, if the system is decaying very slowly, then the check may be unable to detect the decay.

A method of checking stability is also provided by the program. A keystroke (lower case "n") allows the user to perturb the entire system by a random number which can be as large as 3% of the amplitude of each lattice

site. The stability check just described is then automatically put into effect. If the system survives a few perturbations, it can definitely be considered stable.

The program also allows the user to save states of motion at a particular drive frequency and amplitude. The user names the state, thus creating a file of these conditions, which can be put into motion whenever needed.

The magnetically-coupled lattice is simulated by a program called "kiki". It incorporates 60 elements with a damping constant β=0.3, a coupling coefficient c^2=0.9, and an uncoupled frequency ω_o^2=0.1. The time step used during data-taking was 100, which corresponds to 100 steps per response cycle. The relative values of c^2 and ω_o^2 were chosen to roughly approximate the actual lattice. The overall values of c^2 and ω_o^2 were chosen such that the linear frequency of the upper cutoff mode is unity.

IV.B. DRIVE PARAMETER PLANE

We numerically observed steady-state upper cutoff breather solitons by employing a hyperbolic secant initial condition profile predicted by the theory (Sec. II.B.). (The other terms in the theory were neglected.) When a file is started, transients can be seen in the motion before it reaches steady state, particularly at high frequencies. A breather soliton can be clearly seen in the middle third of the display. It exhibits a characteristic skew in its profile (Sec. IV.C.). The system is allowed to reach steady state and then the stability check is actuated for an element in the mid-range of the soliton. The drive amplitude is then incremented up or down with the frequency held constant until the soliton exhibits an instability, and ceases to exist. The minimum and maximum drive amplitudes at which the instabilities occur are recorded. Then the process is repeated for another drive frequency. In this way, we determine over what range of the drive plane the solitons can exist. The results are shown in Fig. IV.B.1.

At the low amplitude boundary, the soliton decays to rest from a finite amplitude. This boundary corresponds to the parametric maintenance condition $\eta \geq \eta_{min}$ where $\eta_{min} = \omega\beta/\omega_0^2$, which follows from $\nu \geq 0$ in (II.C.13). The lower boundary data in Fig. IV.B.1 fall close to the straight line $\eta = \eta_{min}$. This has also been shown to occur for the standard model (Walden 1991).

At the high amplitude boundary, the behavior depends upon the frequency. At low frequencies (ω less than roughly 1.4), the dc "pressure" (Sec. II.B) causes the soliton to "pinch off" in the middle and create two adjacent solitons. This process continues until an extended standing wave is obtained. However, this state is unstable and the lattice soon exhibits no apparent structure. At higher frequencies (ω greater than roughly 1.4), quasiperiodicity occurs. The soliton then becomes highly focused and quickly loses all structure. The final state appears to be one of complete disorder.

It is not known if the drive plane region of the breather is bounded. Indeed, further investigation may reveal new instabilities at higher frequencies.

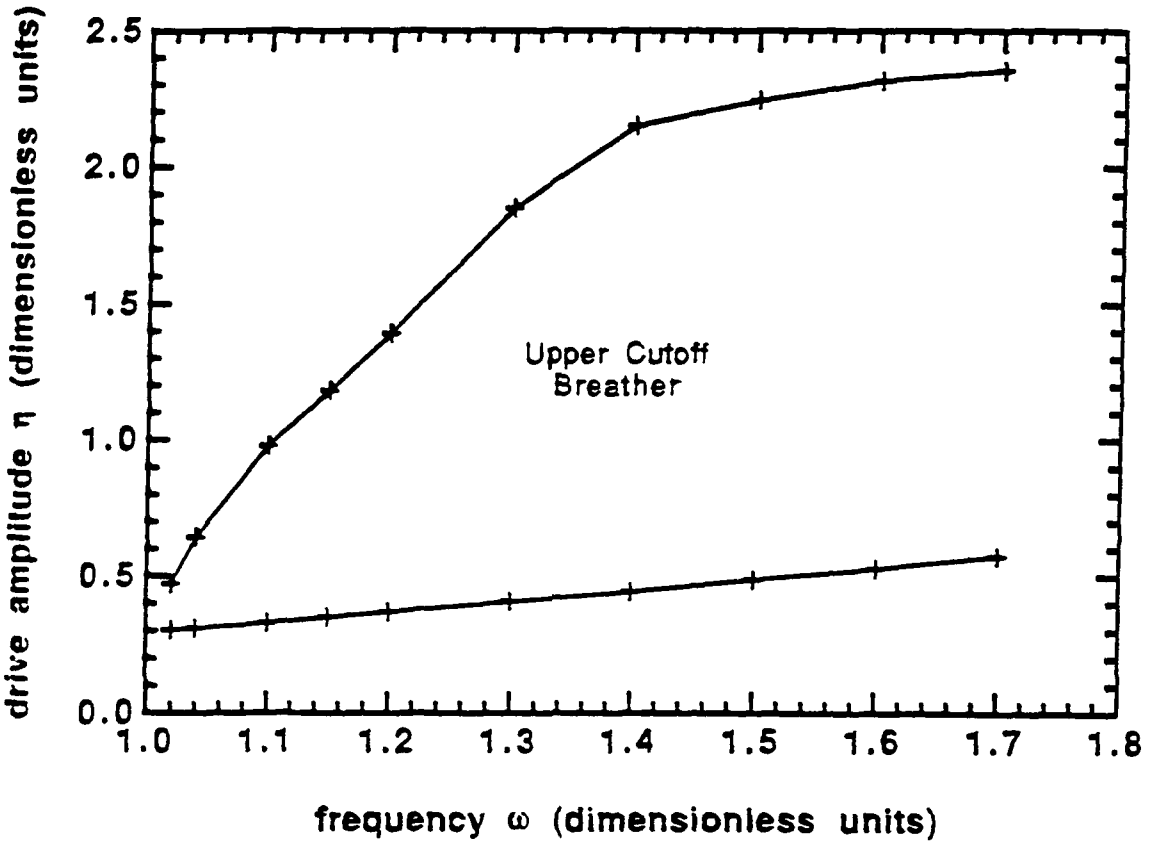

Fig. IV.B.1 Numerical drive parameter plane for the upper cutoff breather. The linear frequency of the upper cutoff mode is unity.

IV.C. COMPARISON TO THEORY

Steady state amplitudes of the oscillators in the numerical simulation were determined for several different breather states. As explained in Sec. II.B, the presence of even-powered nonlinearities causes the minimum and maximum turning point displacements to have different magnitudes, so we determined both of these for each oscillator. The data were then compared to the theoretical predictions (Sec. II.B).

Fig. IV.C.1 shows the results for a low-amplitude breather. The "x" markers represent the numerical turning points at one time, and the "o" markers a half-cycle of the response later (or earlier). The curves represent the approximate theoretical expression (II.B.17). The only adjustable parameter in the theory is the location x_0 of the center of the breather. Numerically, we find that the breather is stable when its center lies halfway between two adjacent lattice sites (location 30.5 in Fig. IV.C.1). The skewness of the numerical data and theoretical curves is apparent. We have seen in Sec. II.B that this is principally the result of the dc component of the motion arising from the quadratic part of the nonlinearity.

In Fig. IV.C.1, the theory only roughly agrees with the numerical data. In fact, the theory is only marginally valid because the largest dc component of the response is comparable to (specifically, about a third) the ac component at that location. Recall that, in order to obtain an analytical solution in Sec. II.B, we assumed that the dc and other frequency components were small compared to the fundamental. The agreement between the theory and numerical data should be better for breathers of still lower amplitude.

Fig. IV.C.2 shows an intermediate amplitude breather. Note that the state is now more localized. Whereas the numerical data show a slight increase in skewness, the effect is very strong in the theoretical curves. These curves have a maximum dc component that roughly equals the ac component, leading

to profiles that are spatially quickly varying. It is questionable if the higher-order terms can successfully describe the smooth numerical data.

Figs. IV.C.3a and IV.C.3b show a high-amplitude breather. Over the region of the drive plane (Fig. IV.B.1) in which the breather exists, the typical structure corresponds overwhelmingly to this case. The numerical data now have a relatively large dc component. Indeed, in the wings of the breather the dc component is an order of magnitude greater than the ac component. At the points of greatest amplitude of the breather, the dc component is roughly twice the ac component. The theory is not expected to be valid, and is seen to completely fail. That the breather continues to exist in this case shows that this localized state is a more general phenomenon than the leading order theory (NLS and lower harmonics) suggests. This point has previously been made in observations of surface wave kinks (Denardo et al. 1990), but the breakdown of the theory is much more dramatic in our case.

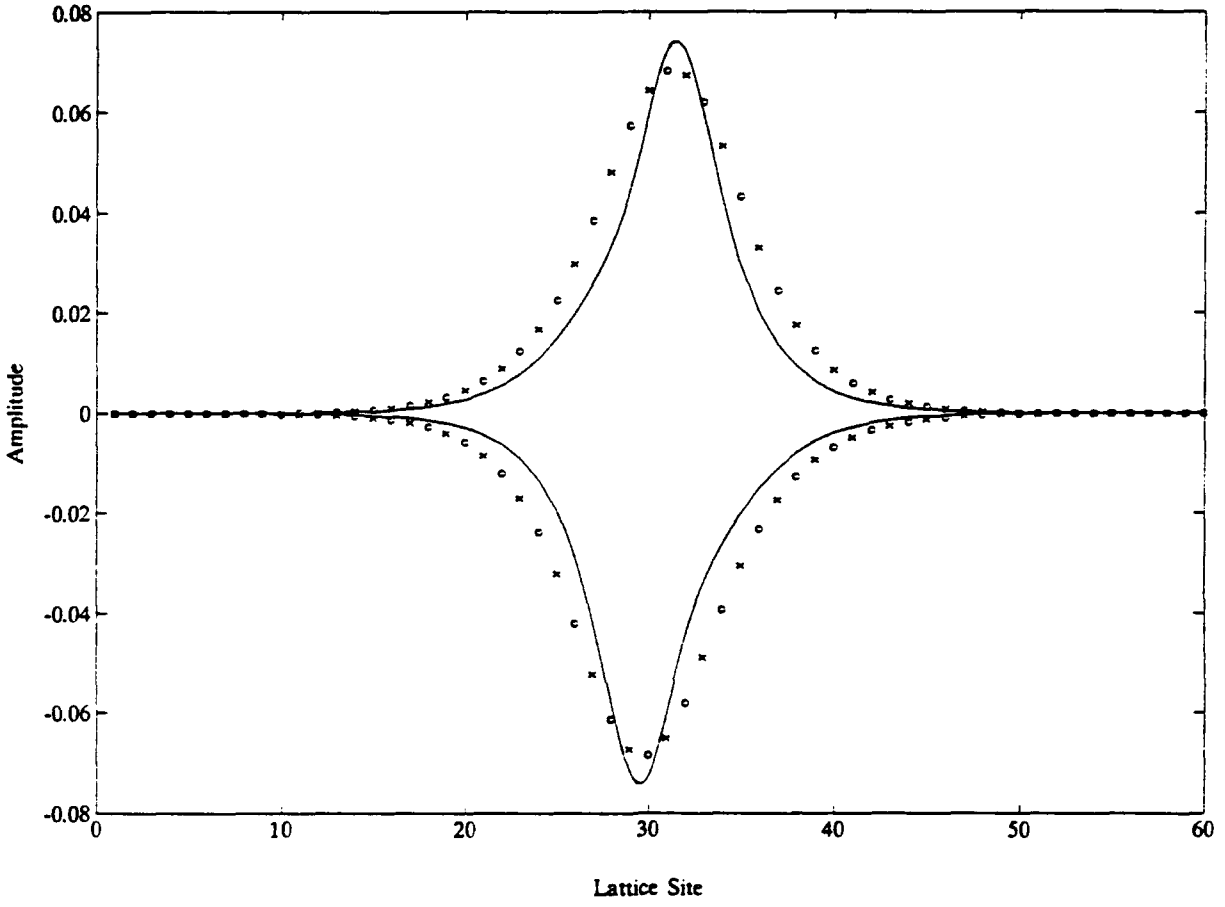

Fig. IV.C.1 Low-amplitude upper cutoff breather. The points are numerical; the curves are from an approximate analytical theory. The drive parameters are ω=1.01 and η=0.32.

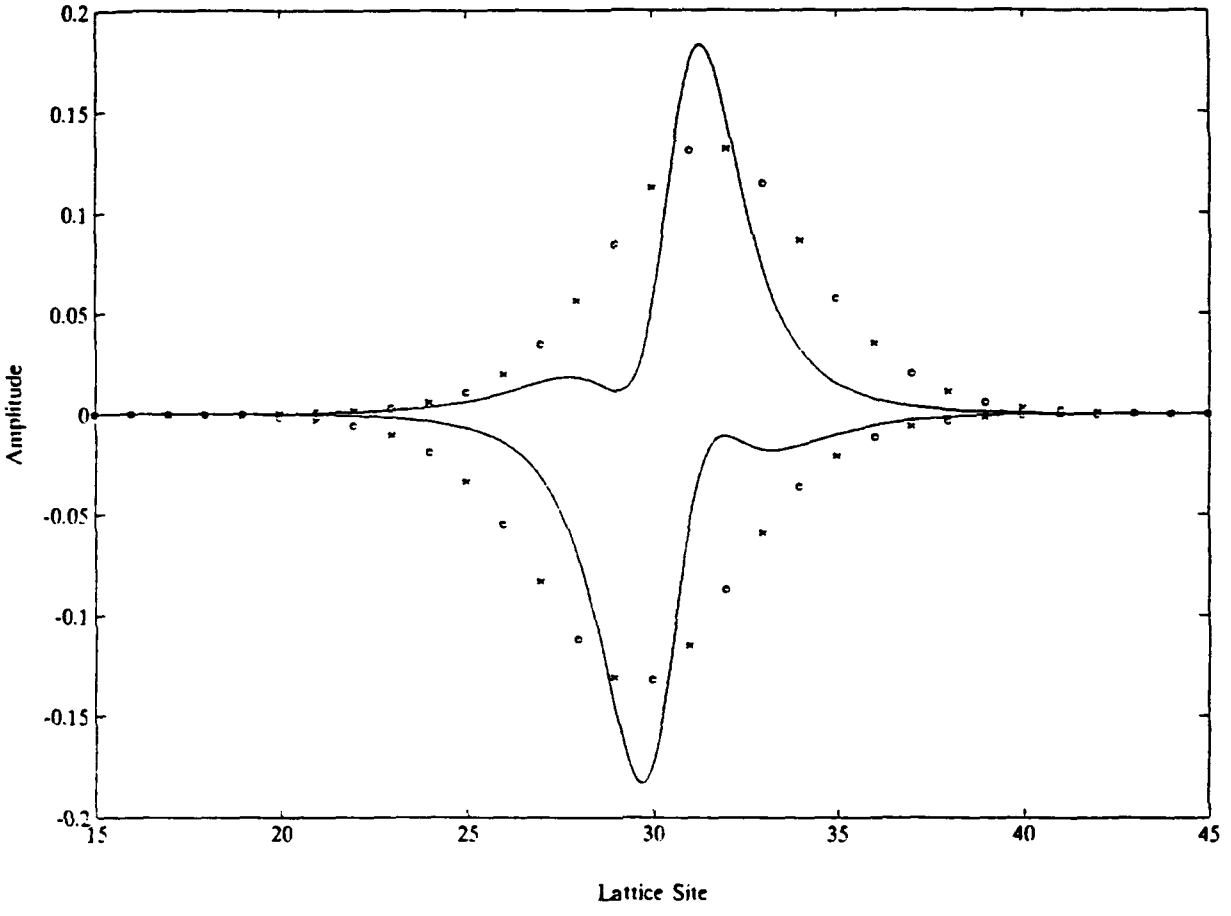

Fig. IV.C.2 Intermediate amplitude upper cutoff breather. The points are numerical; the curves are from an approximate analytical theory. The drive parameters are $\omega = 1.04$ and $\eta = 0.35$.

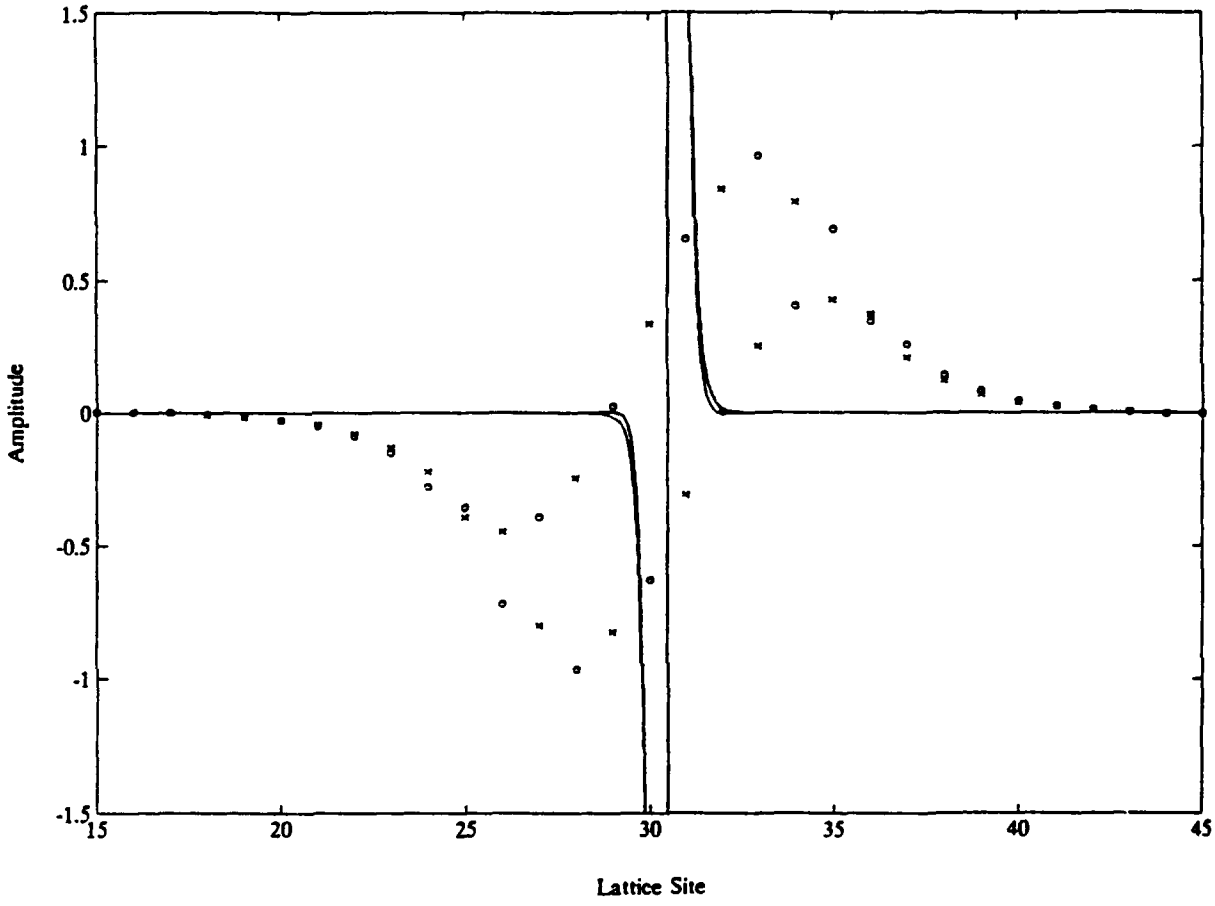

Fig. IV.C.3a High-amplitude upper cutoff breather. The points are numerical; the curves are from an approximate analytical theory. The drive parameters are ω=1.80 anf η=0.90.

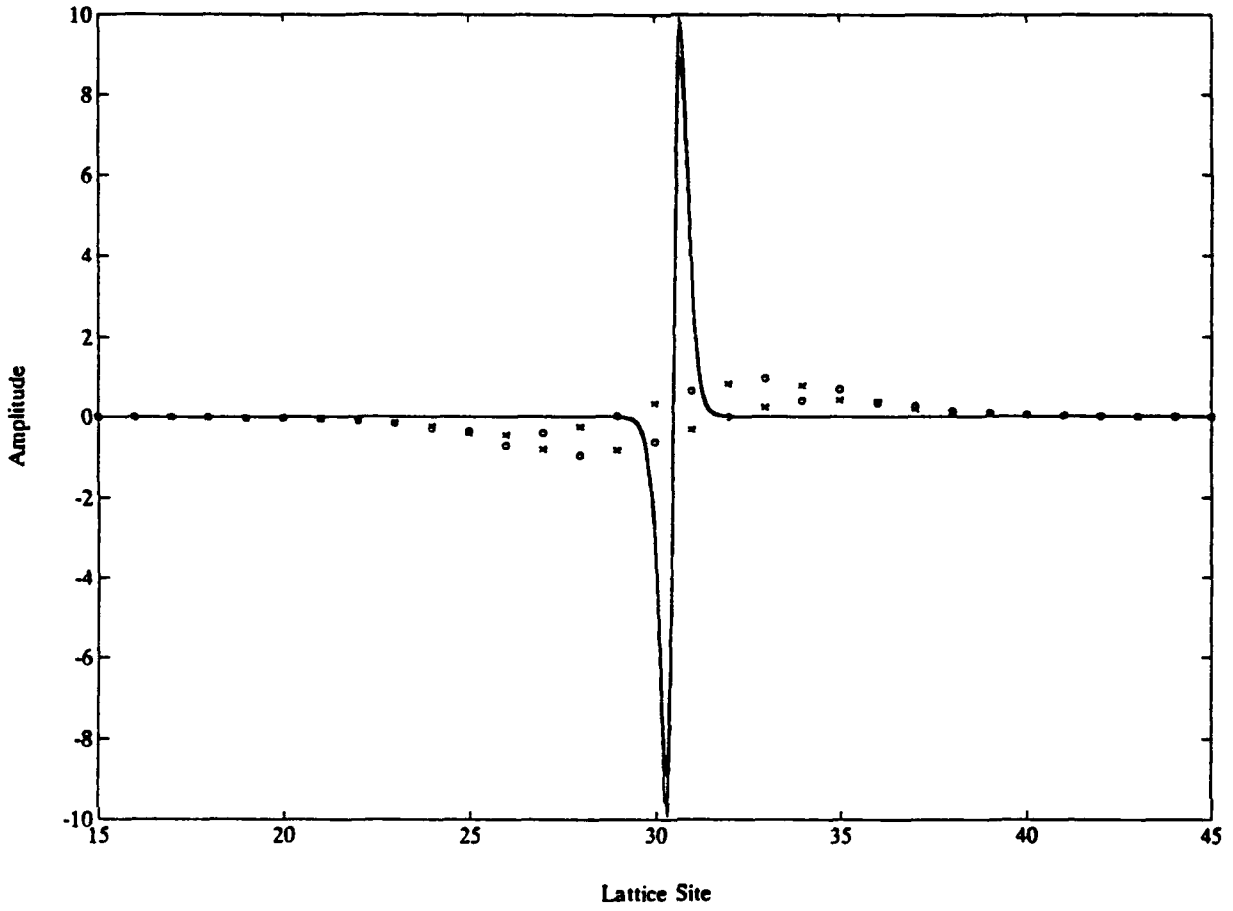

Fig. IV.C.3b Same graph as Fig. IV.C.3a, except that the ordinate is expanded so that the full theoretical curves can be seen.

V. CONCLUSIONS AND FUTURE WORK

Previous workers investigated three of the four nonlinear Schrödinger (NLS) solitons in cutoff modes of vibratory systems. The subject of this thesis is the fourth: the upper cutoff breather. We have observed it experimentally in a lattice of magnetically coupled pendulums, and have numerically simulated it in a simplified model of the actual lattice. These observations are important because they show that the upper cutoff breather can occur in actual systems. Indeed, analytical investigations that predicted the breather are only approximate, so one would wonder about the existence and behavior of the state in real systems.

Our observations yielded a dramatic and unexpected behavior. Except for a very small range of the drive parameters (frequency and amplitude), the breather was not at all described by a hyperbolic secant profile as expected, or even by a single hump. Indeed, for higher drive frequencies and amplitudes the observed skewness is predominant, and can lead to an instability that causes the structure to disentangle into two distinguishable breathers. Analytical investigations showed that the skewness is a result primarily of a dc force that arises from the quadratic part of the nonlinearity. One is accustomed to such "higher order" effects being substantially smaller than the primary "first order" excitation. However, in our system the dc motion was in some cases an order of magnitude greater than the fundamental motion. The theory, being a perturbative approach, completely fails in these cases. It is remarkable that this condition can exist in any system, and that the localized structure continues to exist.

There is a substantial amount of possible future work motivated by this thesis. The current magnet lattice (Ch. III) suffers from static friction effects at low amplitudes. An alternative to pivoting the pendulums has been

suggested by R. Keolian. This employs a flexing thin plastic strip, which would completely eliminate static friction. Such an improvement would be desirable or perhaps necessary for the observation of so-called "soliton-shedding," in which the end of the lattice is driven at a pure frequency and solitons might be ejected at some lower incommensurate frequency. This phenomenon has only been observed in a large surface wave tank (Kit et al. 1987). Recent numerical investigations of nonlinear lattices show that the effect should also be observable in these systems (Walden 1991). This is important because it could lead the way to establishing soliton shedding as fundamental behavior which may occur in a wide variety of systems.

There is another type of excitation that may yield interesting behavior. If wind is arranged to blow along the lattice, waves can be produced. The coupling of the wind to the waves, and the subsequent nonlinear motion of the waves, might offer insightful comparisons and contrasts to wind-generated waves in the ocean.

Several of our lattices that failed to yield breathers have motivated possible research. The interrupted pendulum lattice (App. B) in which cylinders osculate at the top of flexible pendulums has a nonanalytic nonlinearity (Denardo 1991). This turns out to yield a quadratically nonlinear Schrödinger equation, whose nonlinear term is proportional to $|\Psi|\Psi$ rather then $|\Psi|^2\Psi$. Localized structures (breathers and kinks) should also be possible in such systems, by our simple physical reasoning (Ch. I). We believe that the quadratic NLS equation has not been investigated.

The bead lattice (App. C) is interesting as a result of the failure to exhibit breathers. The transverse degeneracy may be responsible. To investigate this, one could constrain the lattice so that there is only one transverse degree of freedom. Alternatively, previous numerical lattice studies (Walden 1991, Galvin 1991) could be generalized to include an additional degree of freedom. The question is then the extent to which this would alter the behavior, or even existence, of the breather. This is of interest in the

possibility of biological solitons, where recent numerical results have shown that an additional degree of freedom in a lattice that models DNA leads to a soliton-initiated separation of the two helices (Muto et al. 1990). DNA indeed undergoes such a transformation in one of its many functions, although the mechanism is not yet known.

APPENDIX A

SINGLE-OSCILLATOR THEORY

In this appendix, we consider some aspects of nonlinear oscillations of single-degree-of-freedom systems. The planar pendulum is employed as the prototype. Free motion is considered in Sec. A.A, where the amplitude-dependent frequency is calculated in the weakly nonlinear limit. Steady state motion in the presence of weak dissipation and weak parametric drive is calculated in Sec. A.B. The results of this appendix are approximately valid for any oscillator whose nonlinearity can be approximated by a force that is cubic in the displacement.

A.A. UNDRIVEN UNDAMPED CASE

Consider the planar pendulum shown in Fig. A.A.1. We assume there is no drive and dissipation. It is not difficult to show that the exact equation of motion for the angular displacement θ is

$$\ddot{\theta} + (g/L)\sin\theta = 0. \qquad \text{(A.A.1)}$$

For small θ, we can approximate $\sin\theta$ by θ, and we get the familiar linear equation of motion of a simple harmonic oscillator:

$$\ddot{\theta} + \omega_0^2\theta = 0\,, \qquad \text{(A.A.2)}$$

where $\omega_0 = \sqrt{\frac{g}{L}}$ is the frequency of oscillation. The period is equal to $2\pi/\omega_0$. Equation (A.A.2) also represents a spring-and-mass system in which the

spring is described by Hooke's law, F=-kx. The general solution to the linear equation (A.A.2) is

$$\theta(t) = A\cos(\omega_o t + \delta) . \qquad \text{(A.A.3)}$$

For arbitrary θ, we can expand $\sin\theta$ in (A.A.1) in a power series:

$$\sin\theta \cong \theta - \frac{\theta^3}{3!} + \frac{\theta^5}{5!} - \ldots . \qquad \text{(A.A.4)}$$

For a weakly nonlinear approximation, we retain only the cubic term in θ. This gives rise to a general nonlinear equation of motion with a cubic nonlinearity:

$$\ddot{\theta} + \omega_o^2 \theta = \alpha\theta^3 . \qquad \text{(A.A.5)}$$

The quantity α is called the nonlinear coefficient. For the pendulum, $\alpha = \omega_o^2/6$.

The dependence of the frequency upon the amplitude for the pendulum can be understood by potential energy considerations. The potential energy of the mass in Fig. A.A.1 is U=mgz , where z is the vertical displacement from the equilibrium position,

$$z = L\,(1 - \cos\theta) . \qquad \text{(A.A.6)}$$

Hence, $$U = mgL(1 - \cos\theta) = 2mgL\sin^2(\theta/2). \qquad \text{(A.A.7)}$$

This is plotted in Fig. A.A.2. For small amplitude, we can make the approximation

$$\sin^2\left(\frac{\theta}{2}\right) \cong \left(\frac{\theta}{2}\right)^2 , \qquad \text{(A.A.8)}$$

so that $U = \left(\frac{mgL}{2}\right)\theta^2$. This is the equation of a parabola and is also plotted in

Fig. A.A.2. Only for small amplitude is the potential energy curve parabolic, which corresponds to linear oscillations.

Based upon the potential energy curve, some qualitative arguments can be made for the dependence of the period on the amplitude. The curve of $U(\theta)$ describes a type of spring for which the restoring force, at large amplitude extension, is less than that for an ideal linear spring at the same extension. Therefore, the period of the oscillation is greater than that of the ideal spring, and the system "softens." Similarly, a spring for which the restoring force is greater than that of the ideal spring at large extension is a "hardening" system. This system will have a smaller period of oscillation than that of the linear spring. The force vs. displacement curves for the linear Hooke's law case as well as the hardening and softening cases are shown in Fig. A.A.3. The linear case corresponds to $\alpha = 0$ in (A.A.5), the softening case to $\alpha > 0$, and the hardening case to $\alpha < 0$.

The dependence of the period of oscillation on the amplitude can be calculated by energy conservation. The exact form of the equation of conservation of energy of the pendulum is

$$\dot{\theta}^2 + 2\omega_0^2 (\cos\theta_o - \cos\theta) = 0, \qquad \text{(A.A.9)}$$

where θ_0 is the maximum angle from equilibrium. The period of oscillation in then given by

$$T = \frac{\sqrt{2}}{\omega_o} \int_{-\theta_o}^{\theta_o} \frac{d\theta}{\sqrt{(\cos\theta - \cos\theta_o)}} . \qquad \text{(A.A.10)}$$

This integral can be solved exactly or by a series expansion of the integrand (French 1971). The result, valid for $\theta_0 << 1$ is

$$T(\theta_o) = T_o\left[1 + \frac{1}{4}\sin^2\left(\frac{\theta_o}{2}\right) + \ldots\right], \qquad \text{(A.A.11)}$$

where the linear period is $T_0 = 2\pi/\omega_0$. To lowest order,

$$T = T_o\left(1 + \frac{\theta_o^2}{16}\right). \qquad \text{(A.A.12)}$$

This gives the dependence of the period of oscillation on the amplitude of motion. In the limit of small θ_0, the equation reduces to $T = T_0$. In terms of the frequency ω, we can express the amplitude dependence, to lowest order, as

$$\omega = \omega_o\left(1 - \frac{\theta_o^2}{16}\right). \qquad \text{(A.A.13)}$$

There is a much simpler and more general way of deriving this weakly nonlinear result. Any oscillatory solution to the equation of motion (A.A.1) must have a Fourier series representation

$$\theta = A\cos\omega t + B\cos 3\omega t + C\cos 5\omega t + \ldots, \qquad \text{(A.A.14)}$$

where we ignore a constant phase. Substituting (A.A.14) into the weakly nonlinear equation of motion (A.A.5) we get

$$[\,4(\omega_o^2 - \omega^2) - 3A^2\alpha\,]\cos\omega t + \{\text{higher harmonics}\} = 0, \qquad \text{(A.A.15)}$$

where the contributions of B, C, . . . to the $\cos\omega t$ term have been neglected because they are small compared to A for weakly nonlinear motion. In order for (A.A.15) to be valid for all time, the coefficients of each independent harmonic must vanish. Setting the coefficient of $\cos\omega t$ equal to zero and solving for ω gives

$$\omega \approx \omega_0 \left(1 - \frac{3\alpha}{8\omega_0^2} A^2\right). \qquad \text{(A.A.16)}$$

For $\alpha = \omega_0^2/6$, this is the same result obtained in (A.A.13) by a much more laborious method.

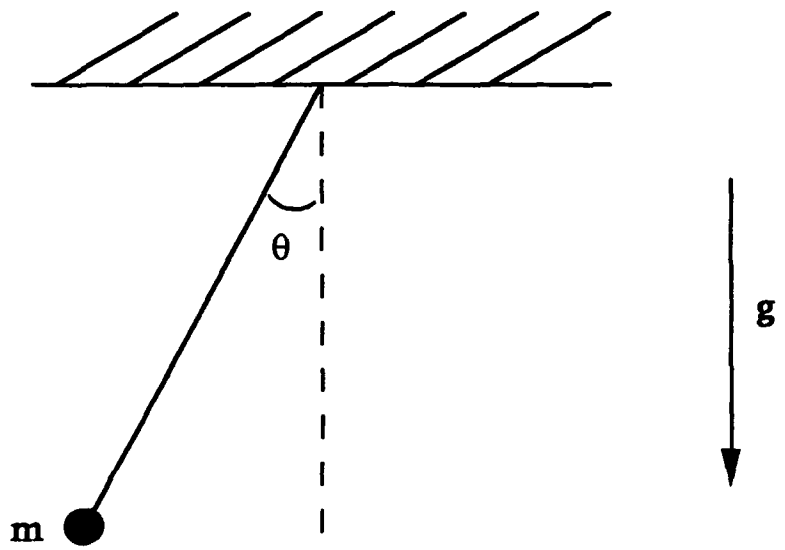

Fig. A.A.1 Planar pendulum.

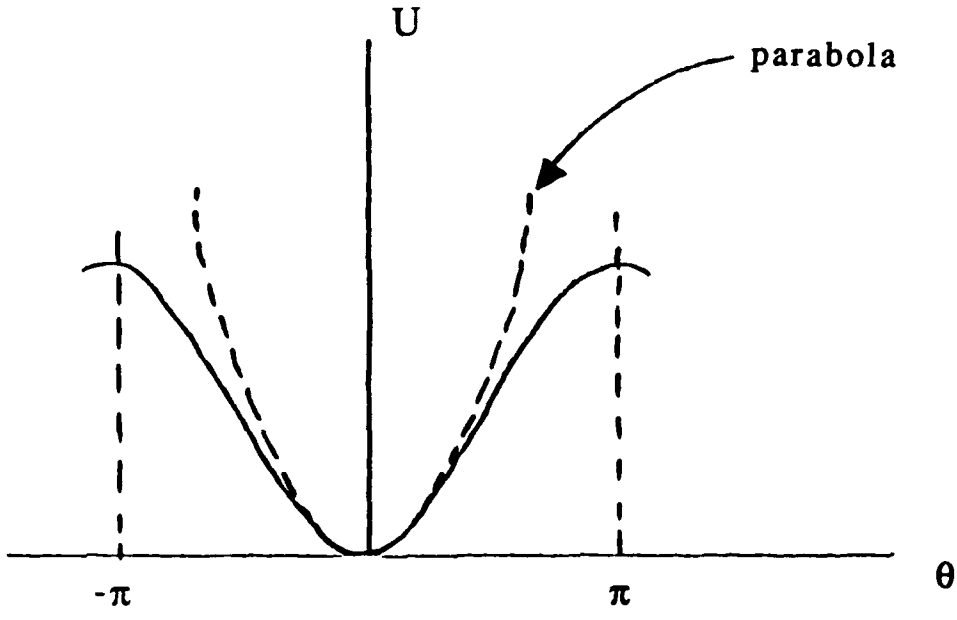

Fig. A.A.2 Potential energy vs. displacement for a pendulum (solid curve).

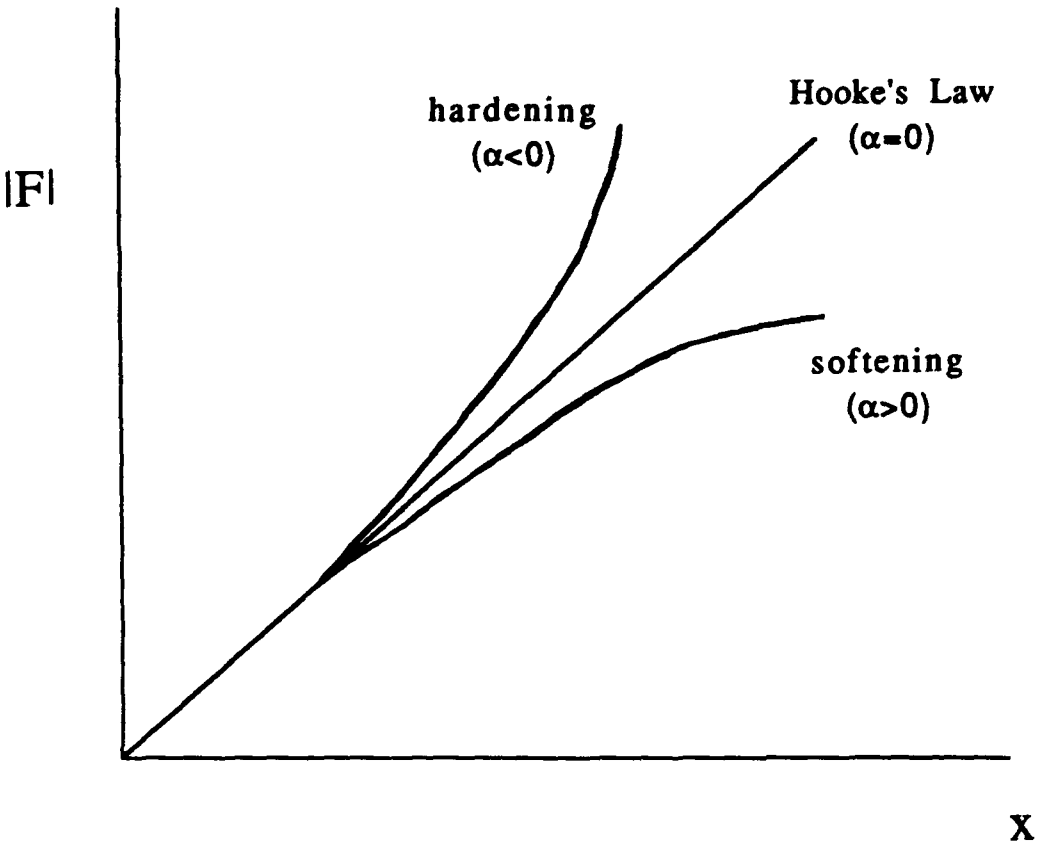

Fig. A.A.3 Force vs. displacement curves for Hooke's law, a hardening system, and a softening system.

A.B. DAMPED PARAMETRICALLY DRIVEN CASE

As discussed in the previous section, the restoring force of a linear oscillator is described by Hooke's law, $F = -kx$, where the "spring constant" k characterizes the stiffness of the force. However, for large |x|, nonlinear effects become important. At large extension, the stiffness may become effectively weaker or stronger than that described by Hooke's law. Thus the system exhibits either hardening (stronger spring constant) or softening (weaker spring constant) for large amplitude motion.

A simple harmonic oscillator will vibrate at maximum amplitude when directly driven at its resonance frequency. The tuning curve (amplitude of response vs. drive frequency for a fixed drive amplitude) for such an oscillator is shown in Fig. A.B.1, where ω_o is the resonance frequency. It is also shown in this figure that for large amplitude motion, the tuning curve bends to the right for a hardening system and to the left for a softening system. This can be easily explained qualitatively. A softening system experiences a weaker restoring force at large amplitude than it would feel if it were perfectly linear. Therefore, the period of the oscillation increases, and resonance occurs at a lower frequency than that of the ideal spring. Similarly, the hardening system feels a stronger restoring force at large amplitude and so the period decreases, and resonance will occur at a higher frequency than that of the ideal spring.

Sufficient bending of the tuning curve causes two stable states to exist over a certain range of drive frequency. This is illustrated by Fig. A.B.2. The part of the tuning curve represented by the broken line corresponds to unstable states, and so these states are never observed. But two stable states of different response amplitudes exist at the same drive frequency over the range between ω_a and ω_b.

We employ a "parametric" rather than direct drive. This refers to a type

of drive that effectively changes some parameter of the system in a periodic manner. In the case of our driven pendulum lattice (Sec. III.A), the effective gravity is being changed as the lattice is shaken up and down. The displacement of the suspension point is

$$d = A\cos\omega_D t \tag{A.B.1}$$

where A is the displacement amplitude of the drive, and ω_D is the drive frequency. The acceleration is thus

$$a = -A\omega_D^2 \cos\omega_D t \tag{A.B.2}$$

The acceleration felt by the lattice is the sum of the constant acceleration due to gravity and the negative of the periodic acceleration due to the drive. This can be expressed as an effective gravitational acceleration

$$g_{eff} = g + A\omega_D^2 \cos\omega_D t\,. \tag{A.B.3}$$

The weakly nonlinear equation of motion of the plane pendulum, including damping and drive, then becomes:

$$\ddot{\theta} + \beta\dot{\theta} + (\omega_o^2 - \frac{A}{L}\omega_D^2\cos\omega_D t)\,\theta = \alpha\theta^3\,, \tag{A.B.4}$$

where β is the damping coefficient and $\alpha=\omega_o^2/6$ for the single plane pendulum. We leave the value of α unspecified in order to obtain more general results. For the principal response of a parametrically driven system, the drive frequency is twice the response frequency, so we set $\omega_D=2\omega$. Furthermore, using an expanded expression for the cosine term in (A.B.4), we obtain

$$\ddot{\theta} + \beta\dot{\theta} + [\,\omega_o^2 - \eta\omega^2\,(e^{i2\omega t} + e^{-i2\omega t})\,]\,\theta = \alpha\theta^3\,, \tag{A.B.5}$$

where $\eta = 2A/L$. If we assume that β, η, and α are small, then any solution to (A.B.5) can be expressed in the form

$$\theta = D(t)\, e^{i\omega t} + \text{c.c.} + \{\text{harmonics}\}\,, \qquad \text{(A.B.6)}$$

where c.c. denotes the complex conjugate, and D(t) is a complex function which varies slowly in time. If the above assumptions are valid, then the harmonics will be small and can be neglected. Substituting (A.B.6) into (A.B.5) and neglecting higher harmonics, we obtain an equation of the form

$$F\, e^{i\omega t} + \text{c.c.} = 0\,, \qquad \text{(A.B.7)}$$

where

$$F = \ddot{D} + \dot{D}(2i\omega + \beta) + D(\omega_0^2 - \omega^2 + i\omega\beta) - D^*\eta\omega^2 - 3\alpha|D|^2 D\,, \qquad \text{(A.B.8)}$$

where D* denotes the complex conjugate of D. Since F is slowly-varying in time and (A.B.7) must be valid for all time, it follows that F must be zero. We can neglect $\ddot{D}$ and $\beta\dot{D}$ because we have assumed that the damping is small and that D is slowly-varying in time. The equation for the complex amplitude D is then

$$\dot{D}(2i\omega) + D(\omega_0^2 - \omega^2 + i\omega\beta) - D^*\eta\omega^2 = 3\alpha|D|^2 D\,. \qquad \text{(A.B.9)}$$

For steady-state motion, D is constant:

$$D = Be^{i\delta}\,, \qquad \text{(A.B.10)}$$

where B and δ are real constants to be determined. Substituting (A.B.10) into (A.B.9), we obtain

$$3\alpha B^2 - \omega_o^2 + \omega^2 - i\omega\beta = -\eta\omega^2 e^{-2i\delta} \ . \qquad \text{(A.B.11)}$$

This equation is equivalent to two real equations and can be solved for the two unknowns, B and δ. The results are

$$B^2 = \frac{1}{3\alpha}\left[\ \omega^2 - \omega_o^2 \pm \omega\sqrt{\eta^2\omega^2 - \beta^2}\ \right] \qquad \text{(A.B.12)}$$

and

$$\tan(2\delta) = \pm \frac{\beta}{\sqrt{\eta^2\omega^2 - \beta^2}} \ . \qquad \text{(A.B.13)}$$

In these solutions, it can be shown that the upper branch is stable and the lower is not (Denardo 1990). Hence, the positive root must be chosen when $\alpha > 0$ (softening), and the negative root when $\alpha < 0$ (hardening).

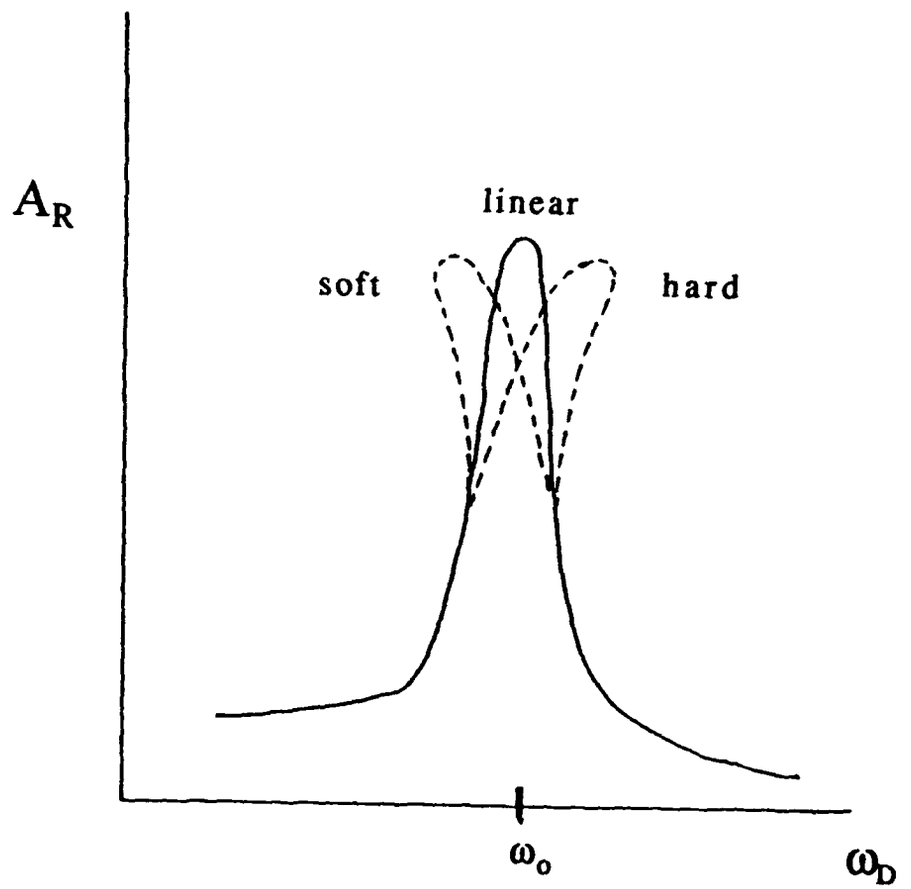

Fig. A.B.1 Response amplitude vs. drive frequency for a linear oscillator, a hardening oscillator, and a softening oscillator.

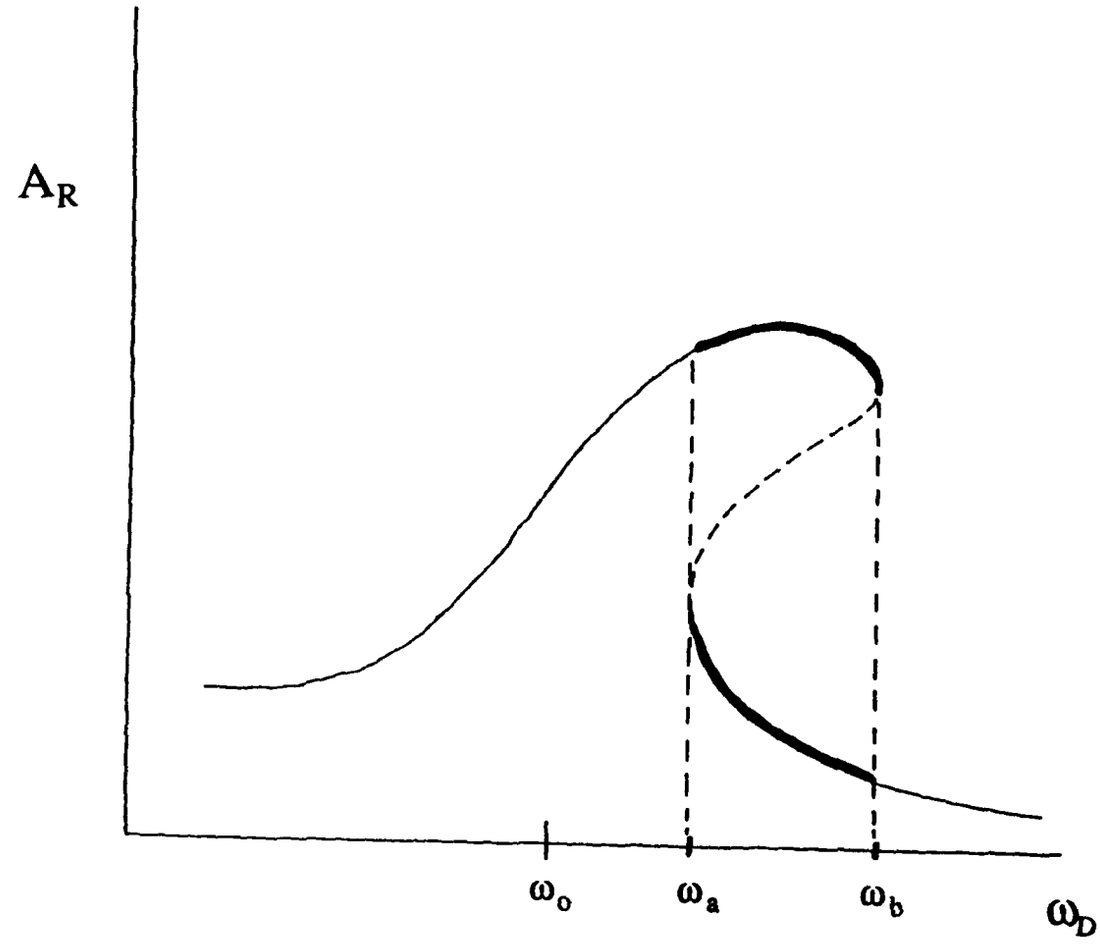

Fig. A.B.2 Tuning curve for a directly driven hardening oscillator.

APPENDIX B

CIRCULARLY-INTERRUPTED LATTICE

One system in which we attempted to observe an upper cutoff breather was a modified pendulum lattice. The lattice was of the string-and-nut type (Denardo 1990). In fact, it was the original such lattice. In order to flip the nonlinearity from softening to hardening, we attached two sections of PVC 4.5 inch outer diameter, 1/4-inch thick pipe (Fig. B.1). These interrupters increasingly shorten the lengths of the pendulums at higher amplitudes, and thus cause hardening. It can be shown that, for the dimensions chosen, this hardening dominates the usual softening due to gravity (Denardo 1991). The cylindrical sections were supported such that there was a small (approximately 1/8-inch) gap where the coupling knots of the lattice were located. (Reducing the gap distance to zero was unacceptable because the coupling between pendulums would vanish.)

An abrupt-nonlinear upper cutoff breather (Fig. B.2) was observed in the lattice at a drive frequency of 8.15 Hz, which is greater than twice the linear upper cutoff frequency of 4.05 Hz. By "abrupt-nonlinear" we mean that the pendulums in motion struck the interrupters whereas the essentially motionless pendulums did not. There was a definite division between the two types, as shown in Fig. B.2. Furthermore, the number of pendulums in motion was adjustable by hand, and the profile was flat as shown. The structure is thus not profound. Indeed, it is clearly very similar to the uninteresting situation of uncoupled oscillators with an abrupt nonlinearity. An exception occurs when many oscillators are in motion; in this case the coupled lattice is subject to the Benjamin-Feir instability (Denardo 1990). The problem is the gap between the cylinders. This, however, is necessary if the coupling is to remain. The lattice is thus fundamentally flawed. This was suspected from the beginning, but we nevertheless decided to proceed due to the quickness with which the modifications could be made.

There is a possible future for a circularly-interrupted lattice, however, which was motivated by our observation of a stable lower cutoff mode in the lattice in Fig. B.1. The stability arises from the fact that the mode now hardens rather than softens, and is thus no longer subject to the Benjamin-Feir instability. Kinks should therefore be possible in this mode, analogous to the shallow-liquid surface wave case (Denardo et al. 1990). To observe these in a lattice, it would be best to have the cylinders osculate at a point above the coupling knots (Fig. B.3). This point would then become the point of support. In this geometry, note that the upper cutoff mode would again have an abrupt nonlinearity that arises for motion of sufficiently large amplitude.

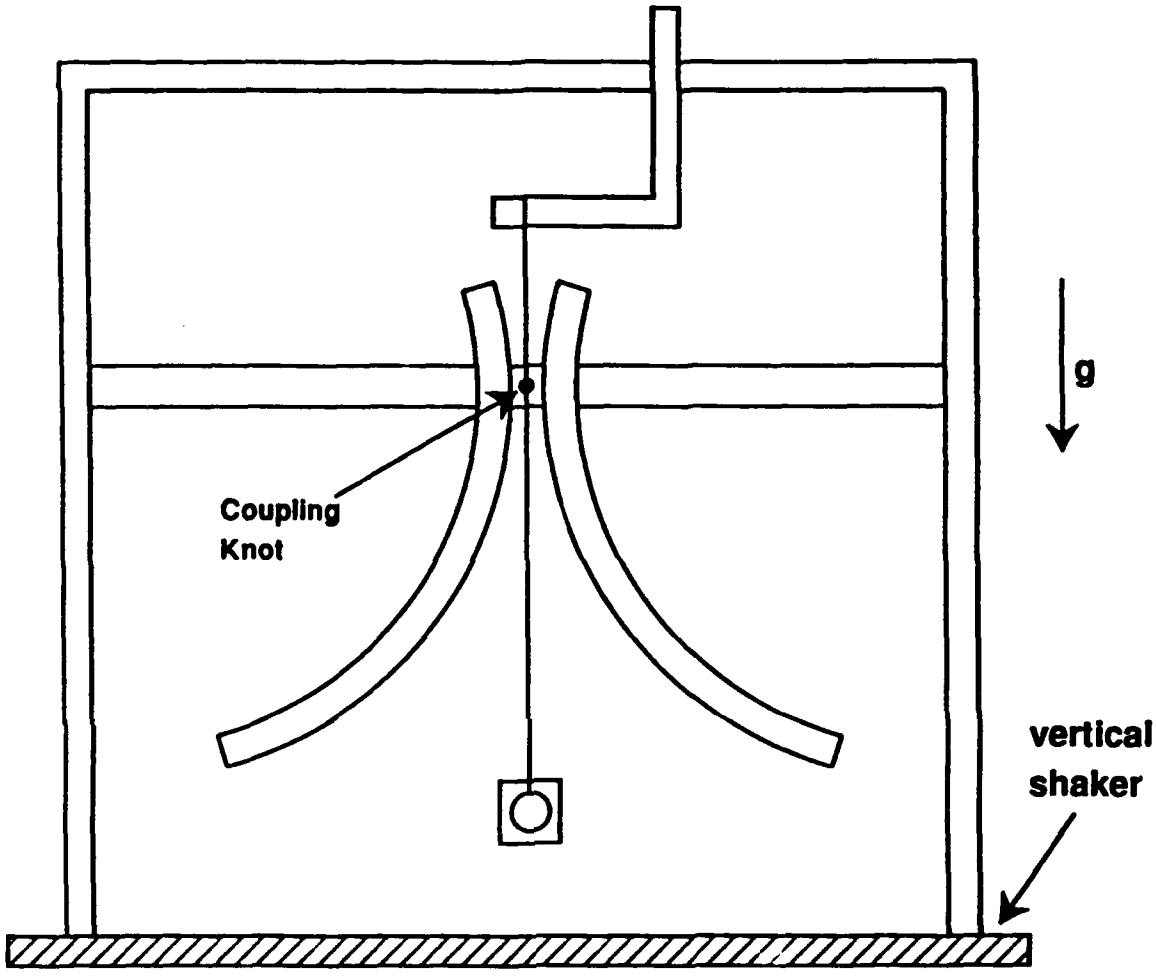

Fig. B.1. Side view of the lattice modified with circular interrupters, which cause the upper cutoff mode to harden.

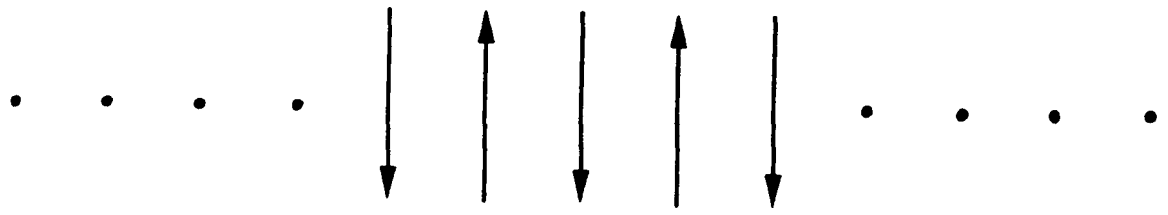

Fig. B.2 Approximate representation of an abrupt-nonlinear breather observed in the circularly interrupted lattice.

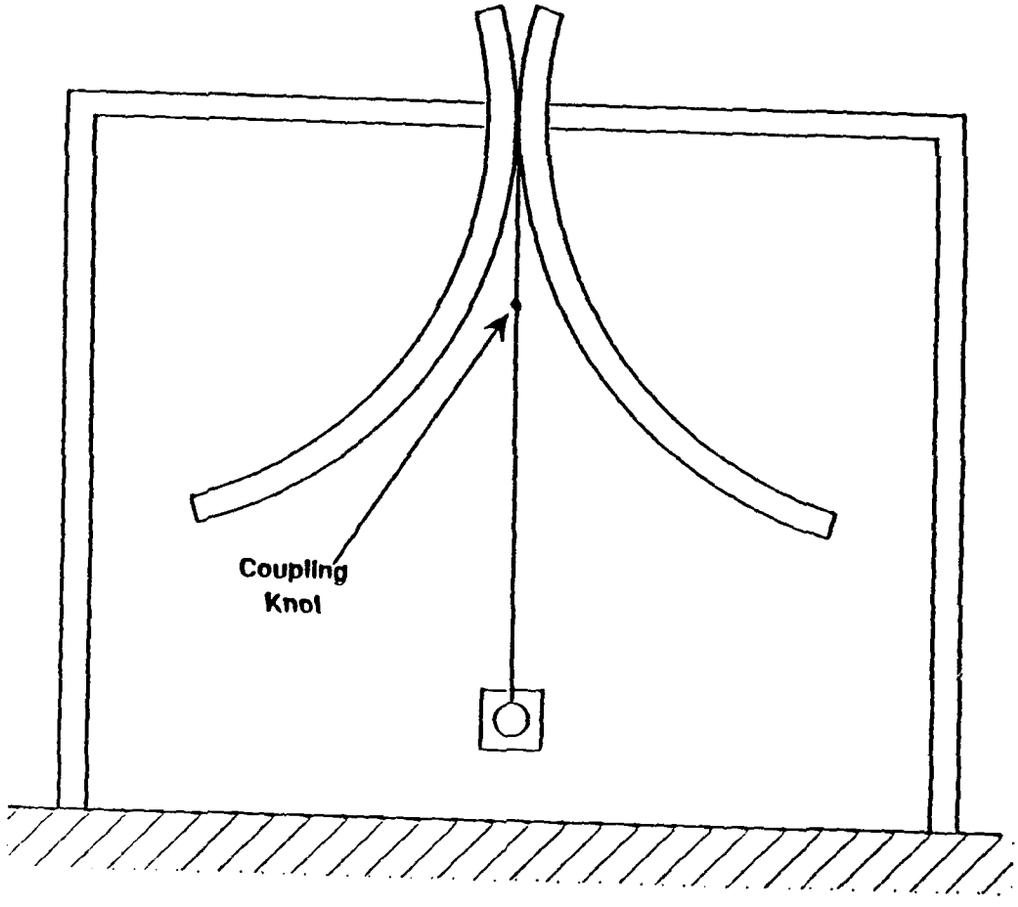

Fig. B.3. Side view of arrangement for a hardening lower cutoff mode, in which kinks should be observable.

APPENDIX C
BEAD LATTICE

One of the lattices in which we attempted but failed to observe upper cutoff breather solitons was a lattice of equally spaced masses on a flexible string under tension. The condition that the transverse upper cutoff mode possess the requisite nonlinear hardening is derived in Sec. C.A. The feasibility of an end-driven arrangement is examined in Sec. C.B, and the experiment is discussed in Sec. C.C. The failure to observe the breathers is interesting because they should exist in such lattices. We suspect that the two-fold degeneracy of transverse motion was responsible for the failure.

C.A. CONDITION FOR HARDENING

In this section, we determine the condition for hardening of the transverse upper cutoff mode of a bead lattice. We achieve this by deriving the equation of motion and requiring the nonlinear coefficient to have the appropriate sign.

Consider a uniform lattice of beads of mass m and lattice spacing a on a perfectly flexible massless string under tension T_0 in equilibrium (Fig. C.A.1). The upper cutoff mode is illustrated in Fig. C.A.2, and a force diagram for a single mass is shown in Fig. C.A.3. We assume that the lattice does not suffer any dc contraction; i.e., that the longitudinal distance between successive masses is always a. From Fig.C.A.3, the net force on a mass is

$$F = -2T\sin\theta\,, \qquad \text{(C.A.1)}$$

where the instantaneous tension in the string is

$$T = T_o + \frac{2YA}{a}\left(L - \frac{a}{2}\right), \qquad \text{(C.A.2)}$$

where Y is Young's modulus and A is the cross-sectional area of the string.

One method of attack is to expand the force F to third order in θ. However, when $\ddot{y}$ is expressed in terms of θ, there appear terms proportional to $\dot{\theta}^2\ddot{\theta}$ and $\theta\dot{\theta}^2$. To determine the hardening condition, one must then substitute the leading order solution into these terms. It is more direct to use the variable y rather than θ. We will employ this approach. Let $\varepsilon=2y/a$ be a small quantity. Then

$$L = \sqrt{\frac{1}{4}a^2 + y^2} = \frac{a}{2}\sqrt{1+\varepsilon^2} \cong \frac{a}{2}\left(1 + \frac{1}{2}\varepsilon^2\right), \qquad \text{(C.A.3)}$$

where the final expression is valid to third order in ε. Furthermore,

$$\sin\theta = \frac{y}{L} = \frac{a\varepsilon}{2L} \cong \frac{\varepsilon}{1 + \frac{1}{2}\varepsilon^2} \cong \varepsilon\left(1 - \frac{1}{2}\varepsilon^2\right). \qquad \text{(C.A.4)}$$

Substituting (C.A.2), (C.A.3), and (C.A.4) into (C.A.1), we find

$$F = -2\left(T_o + \frac{YA}{2}\varepsilon^2\right)\left(\varepsilon - \frac{1}{2}\varepsilon^3\right). \qquad \text{(C.A.5)}$$

To third order in ε, the equation of motion for the upper cutoff mode is thus

$$\ddot{\varepsilon} + \omega_o^2\varepsilon = \alpha\varepsilon^3, \qquad \text{(C.A.6)}$$

where the square of the linear frequency of motion is

$$\omega_o^2 = \frac{4T_o}{ma}, \qquad \text{(C.A.7)}$$

and the nonlinear coefficient is

$$\alpha = -\frac{2}{ma}\left(YA - T_o\right). \qquad \text{(C.A.8)}$$

On the nonlinear level, there is competition between the geometry (which tends to soften the oscillations) and the amplitude-dependent tension (whose increase tends to harden the oscillations). From (C.A.8), the condition $\alpha<0$ for hardening is

$$YA > T_0. \qquad \text{(C.A.9)}$$

In the next section, we will consider the feasibility of satisfying this condition, along with the condition of a global parametric drive.

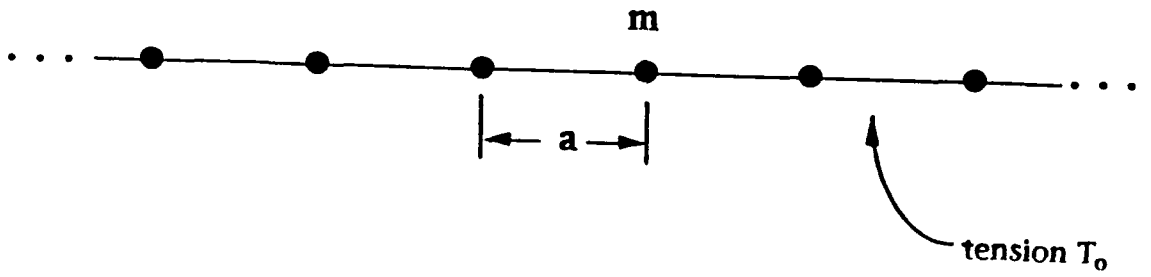

Fig. C.A.1 Uniform lattice of beads on a string. We consider transverse motion.

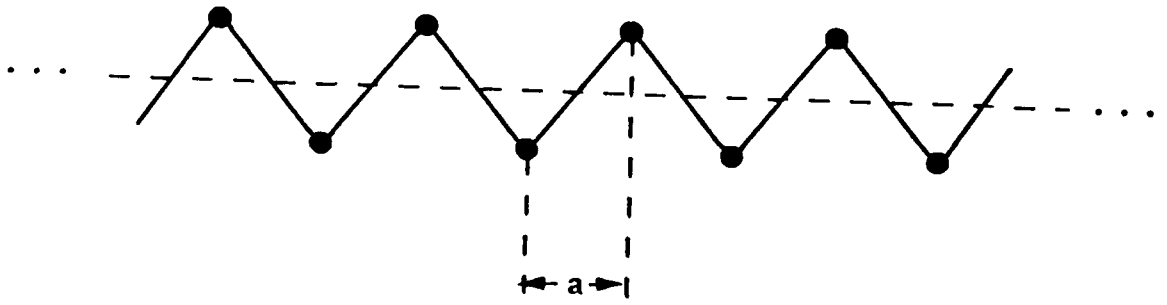

Fig. C.A.2 Upper cutoff mode of the bead lattice in Fig. C.A.1.

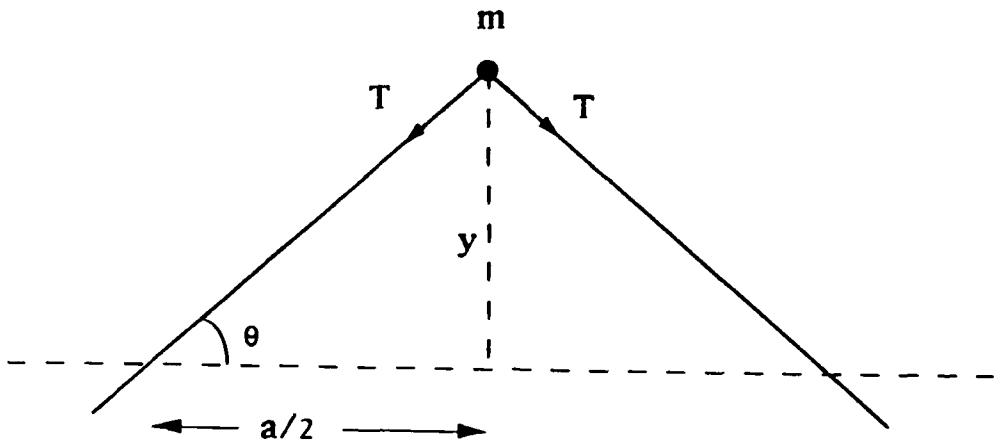

Fig. C.A.3 Force diagram for a single mass of the lattice undergoing upper cutoff motion.

C.B. CONDITION FOR GLOBAL PARAMETRIC DRIVE

We will now determine the condition for global parametric drive of the bead lattice driven at one end. By "global" we mean spatially uniform. Consider a uniform lattice of beads of mass m and spacing a on a perfectly flexible massless string of length L and under tension T_0. The tension is modulated by a longitudinal drive at one end of the string (Fig. C.B.1). The drive frequency is 2ω, where ω is approximately equal to ω_b, the linear frequency (C.A.7) of the upper cutoff mode. Our problem is to determine the condition for which the modulation of the tension (or the stretching of the string) is approximately uniform with regard to the time scale of transverse oscillations.

The square speed of longitudinal waves in an elastic medium is

$$c^2 = \frac{Y}{\rho}, \tag{C.B.1}$$

where Y is Young's modulus and ρ is the mass per unit volume. For the bead lattice in the continuum limit,

$$\rho = \frac{m}{aA} \tag{C.B.2}$$

where A is the cross-sectional area of the string. Hence,

$$c^2 = \frac{Y}{\rho} = \frac{YAa}{m} . \tag{C.B.3}$$

This is the square speed of longitudinal waves in the lattice if the wavelength is much greater than a. The time required for such a wave to travel the length of the lattice is L/c. For the drive to be global, this time must be short compared to the period $2\pi/\omega_0$ of oscillations, where ω_0 is given by (C.A.7) We

thus require $L/c << 2\pi/\omega_0$, or

$$c^2 >> \frac{\omega_o^2 L^2}{4\pi^2} . \qquad \text{(C.B.4)}$$

Substituting (C.B.3) and simplifying, we arrive at the global drive condition

$$YA >> \frac{L^2 T_o}{a^2 10} = \frac{N^2 T_o}{10} , \qquad \text{(C.B.5)}$$

where N is the total number of beads. The condition for hardening is $YA > T_o$ (C.A.9). Hence, if we satisfy the global drive condition (C.B.5) then we automatically satisfy the hardening condition.

Our global drive condition is stringent. The weakest possible condition is to have the time required for a longitudinal wave to pass one lattice spacing be small compared to a period. This is equivalent to

$$c_l^2 >> c_\perp^2 , \qquad \text{(C.B.6)}$$

where the square longitudinal speed is

$$c_l^2 = c^2 = \frac{YAa}{m} , \qquad \text{(C.B.7)}$$

and the square transverse speed is

$$c_\perp^2 = \frac{\omega_o^2}{k^2} = \frac{4T_o a}{\pi^2 m} . \qquad \text{(C.B.8)}$$

This leads to the global drive condition

$$YA >> \frac{2T_o}{5} , \qquad \text{(C.B.9)}$$

which is weaker than (C.B.5). If (C.B.9) is satisfied, note that the hardening condition (C.A.9) is again automatically satisfied.

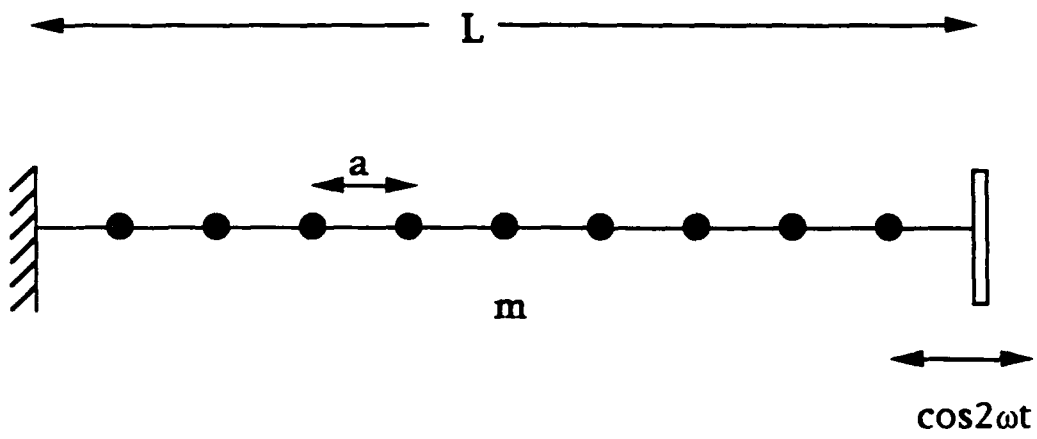

Fig. C.B.1 Uniform lattice of beads on a string with a sinusoidally-driven boundary.

C.C. EXPERIMENT

A bead lattice was constructed with 14-lb test 0.35 mm diameter monofilament nylon (fishing line), to which 30 1.8-gram lead "sinkers" were crimped 10.2 cm apart. To ensure a high degree of uniformity, we selected sinkers whose masses were within ± 0.3% of the average value. One end of the lattice was attached to a heavy duty eyelet that was screwed into an anchor implanted in the concrete ceiling of the laboratory. The other end was attached to an aluminum frame that was fixed to a shaker that rested on the floor. We arranged the tension in the lattice to be roughly known by temporarily disconnecting it from the frame and attaching a known hanging weight (1kg) to the bottom. The nylon was then clamped to the frame, after which the weight was removed. We selected boundary conditions appropriate for the upper cutoff mode: the ends were located one-half of a lattice spacing from the nearest beads.

It should be noted that, because the bead lattice is vertical, the tension is not constant. Rather, it increases with downward distance. The difference in tension between the top and bottom is the total weight of the beads (the mass of the nylon is negligible), which corresponds to 30 x 1.8 gram = 0.054 kg. This amounts to roughly a 5% change, which we consider to be acceptable.

The product YA of the Young's modulus and cross-sectional area of the nylon was determined in an independent experiment that was suggested and arranged by D. Gardner. A known mass was suspended from the end of a sample of known length of nylon, and the frequency of oscillations was measured with an accelerometer. This yielded YA=445 N, which is the weight of 45 kg.

To accurately determine the linear upper cutoff frequency f, we measured the linear frequency f_0 of the fundamental. This gave f_0=3.28 Hz, which implies a tension T=7.2 N (or 0.73 kg). The relationship between the

frequencies can be shown to be $f_1=(2N/\pi)f_0$, from which the drive frequency corresponding the the upper cutoff mode is found to be $2f_1=125$ Hz.

We drove the lattice at this value and at a variety of frequencies above and below this value, and at a variety of amplitudes. No localized states were observed. The transverse oscillations of the masses were clearly two-dimensional. It may be that this degeneracy prevents the formation of breathers.

LIST OF REFERENCES

Christiansen, P., 1988, "Observations of Real Solitons," Nature, 332, 12-13.

Davydov, A., 1985, Solitons in Biological Systems, Reidel, Boston.

Denardo, B., 1990, Observations of Nonpropagating Oscillatory Solitons, Ph. D. Dissertation, University of California, Los Angeles.

Denardo, B., 1991, "Nonlinear Oscillations of Circularly Interrupted Pendulums," unpublished.

Denardo, B., Galvin, B., Greenfield, A., Larraza, A., Putterman, S. and Wright, W., 1992, "Observations of Localized Structures in Nonlinear Lattices: Domain Walls and Kinks," Phys. Rev. Lett. 68, 1730-1733.

Denardo, B., Wright, W., Putterman, S., and Larraza, A., 1990, "Observation of a Kink Soliton on the Surface of a Liquid," Phys. Rev. Lett. 64, 1518-1521.

Dodd, R., Eilbeck, J., Gibbon, J. and Morris, H., 1982, Solitons and Nonlinear Wave Equations, Academic Press.

Feynman, R., Leighton, R., and Sands, M., 1965, Lectures on Physics, Vol. III, Addison-Wesley, Sec. 13, p. 12.

French, A. P., 1971, Newtonian Mechanics, W. W. Norton & Company, p. 434-442.

Galvin, B., 1991, Numerical Studies of Localized Vibrating Structures in Nonlinear Lattices, Master's Thesis, Naval Postgraduate School, Monterey, California.

Kit, E., Shemer, L., and Miloh, T., 1987, "Experimental and Theoretical Investigation of Nonlinear Sloshing Waves in a Rectangular Channel," J. Fluid Mech. 181, pp. 265-291.

Larraza, A. and Putterman, S., 1984a, "Theory of nonpropagating hydrodynamic solitons," Phys. Rev. Lett. 103A, 15-18.

Larraza, A. and Putterman, S., 1984b, "Theory of nonpropagating surface wave solitons," J. Fluid Mech. 148, 443-449.

Miles, J., 1984, "Parametrically excited solitary waves," J. Fluid Mech., 148, 451-460.

Mollenauer, L. F., Gordon, J. P. and Evangelides, S. G., 1991, "Multigigabit Soliton Transmissions Transverse Ultralong Distances," Laser Focus World, Nov., pp. 159-170.

Muto, V., Lomdahl, P., Christiansen, P., 1990, "A Two-Dimensional Discrete Model for DNA Dynamics: Longitudinal Wave Propagation and Denaturation," Phys. Rev. A. 42. 7452.

Walden, C., 1991, Numerical Investigations of Breather Solitons in Nonlinear Vibratory Lattices, Master's Thesis, Naval Postgraduate School, Monterey, California.

Wu, J., Keolian, R., and Rudnick, I., 1984, "Observation of a Nonpropagating Hydrodynamic Soliton," Phys. Rev. Lett. 52, 1421-1424.

Zabusky, N. and Kruskal, M., 1965, "Interaction of 'solitons' in a collisionless plasma and the recurrence of initial states," Phys. Rev. Lett. 15, 240-243.

INITIAL DISTRIBUTION LIST

1.	Defense Technical Information Center Cameron Station Alexandria, Virginia 22304-6145	2
2.	Library, Code 052 Naval Postgraduate School Monterey, California 93943-5002	2
3.	Dr. Bruce Denardo Physics Department, PH/De Naval Postgraduate School Monterey, California 93943-5002	4
4.	Professor Steven Garrett Physics Department, PH/Gx Naval Postgraduate School Monterey, California 93943-5002	1
5.	Professor Andrés Larraza Physics Department, PH/La Naval Postgraduate School Monterey, California 93943-5002	2
6.	Professor Karlheinz Woehler, Chairman PH Physics Department Naval Postgraduate School Monterey, California 93943-5002	1
7.	Mary L. Atchley Physics Department Naval Postgraduate School Monterey, California 93943-5002	2
8.	Professor Seth Putterman Physics Department University of California Los Angeles, California 90024-1547	1